nature cell biology

RESOURCE

A genomic toolkit to investigate kinesin and myosin motor function in cells

Zoltan Maliga[1,8], Magno Junqueira[2,7], Yusuke Toyoda[1,7], Andreas Ettinger[3], Felipe Mora-Bermúdez[1], Robin W. Klemm[4], Andrej Vasilj[1], Elaine Guhr[1], Itziar Ibarlucea-Benitez[5], Ina Poser[1], Ezio Bonifacio[6], Wieland B. Huttner[1], Andrej Shevchenko[1] and Anthony A. Hyman[1]

Coordination of multiple kinesin and myosin motors is required for intracellular transport, cell motility and mitosis. However, comprehensive resources that allow systems analysis of the localization and interplay between motors in living cells do not exist. Here, we generated a library of 243 amino- and carboxy-terminally tagged mouse and human bacterial artificial chromosome transgenes to establish 227 stably transfected HeLa cell lines, 15 mouse embryonic stem cell lines and 1 transgenic mouse line. The cells were characterized by expression and localization analyses and further investigated by affinity-purification mass spectrometry, identifying 191 candidate protein–protein interactions. We illustrate the power of this resource in two ways. First, by characterizing a network of interactions that targets CEP170 to centrosomes, and second, by showing that kinesin light-chain heterodimers bind conventional kinesin in cells. Our work provides a set of validated resources and candidate molecular pathways to investigate motor protein function across cell lineages.

Actin and microtubules define polarized and dynamic cytoskeletal networks required for cell integrity, intracellular transport and faithful cell division. An important class of proteins that works together with these polymer systems is the structurally related, P-loop motor protein superfamily[1]. The human genome contains 39 myosin and 44 kinesin genes but the exact number varies widely across eukaryotes[2,3]. Gene targeting *in vivo*[4–6], RNA-mediated interference (RNAi) analysis[7–9] and biochemical approaches[10–12] have provided insights into the generic functional roles for a number of motors. However, at present, there is no resource available that allows a comprehensive analysis of motor function in a given cell type or to trace the changes of a motor-specific activity across cell-fate transitions. Bacterial artificial chromosome (BAC) transgenes provide an ideal platform for high-throughput analysis of gene function in cultured cells and *in vivo*[13,14]. This is because BACs contain the gene together with many *cis*-regulatory sequences required for native control of gene expression, the production of relevant isoforms and proper translational control through the cell cycle. Targeted recombination in *Escherichia coli* can be used to insert tagging cassettes or substitute nucleotide residues in its genomic context[15,16]. Therefore, once stably integrated, the resulting BAC transgenes can be expressed under their native promoter and orthologous transgenes can be used as RNAi-resistant third alleles[15,17]. Indeed, these methods have successfully generated resources to study the interplay between mitotic genes[13], to characterize all components of a cellular organelle (the centrosome)[18], to generate a genome-wide histone methylation map[19] and to perform targeted studies of individual proteins[15,20,21].

Here, we generate a transgeneOmics resource for motor proteins to investigate 71 of the 82 annotated human kinesin and myosin genes. Stable transfection of BACs generated 227 HeLa cell and 15 mouse embryonic stem cell (mESC) lines. To further show that this resource is readily adaptable to *in vivo* experiments, we established a transgenic mouse line expressing recombinant human KIF23. We report localization patterns for previously uncharacterized motor proteins in HeLa cells and define candidate protein–protein interactions identified by systematic affinity-purification mass spectrometry (AP–MS) from transgenic HeLa cell lysates. We illustrate the use of our resource with two discoveries: a mechanism that regulates centrosome composition and a previously unknown light-chain organization in conventional kinesin.

[1]Max-Planck Institute for Cell Biology and Genetics (CBG), Dresden 01307, Germany. [2]Brazilian Center for Protein Research, Department of Cell Biology, University of Brasilia, 70910-900 Brasilia, DF, Brazil. [3]Department of Cell and Tissue Biology, University of California, San Francisco, San Francisco, California 94143, USA. [4]Department of Cell Biology, Harvard Medical School, Boston, Massachusetts 02115, USA. [5]Department of Molecular and Cell Biology, University of California, Berkeley, Berkeley, California 94720, USA. [6]Center for Regenerative Therapies Dresden, Technische Universität Dresden, Dresden 01307, Germany. [7]These authors contributed equally to this work.
[8]Correspondence should be addressed to Z.M. (e-mail: maliga@mpi-cbg.de)

Received 21 August 2012; accepted 10 January 2013; published online 17 February 2013; DOI: 10.1038/ncb2689

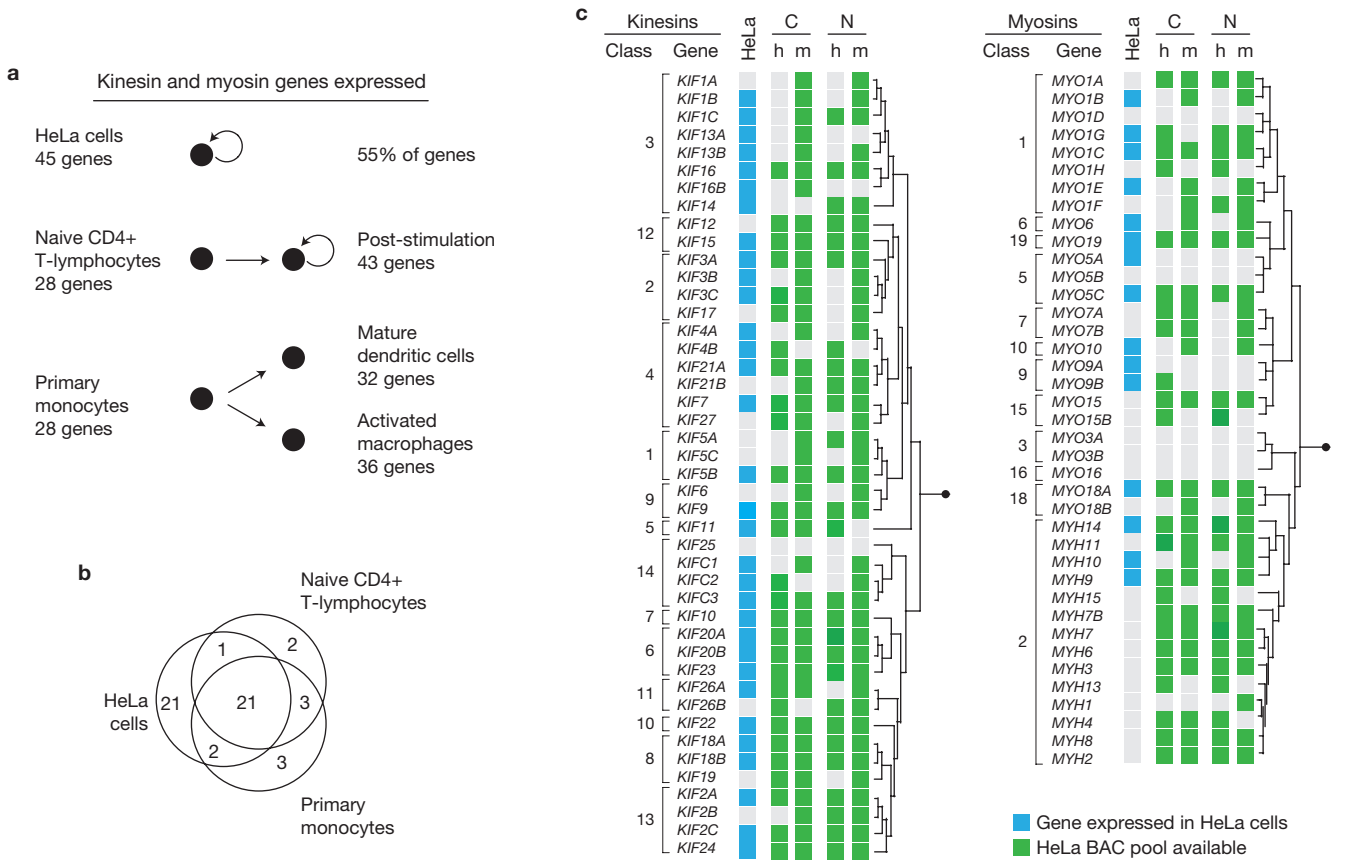

Figure 1 Towards a comprehensive motor transgene collection in HeLa cells. (**a**) The number of kinesin and myosin genes expressed in HeLa cells or human immunocytes measured by microarray transcription profiling in biological triplicate (see Supplementary Table S1). Arrows connecting two cell types indicate *ex vivo* differentiation. Curved arrows indicate cell proliferation. (**b**) Venn diagram comparing motor gene expression in HeLa cells and two primary human immune cell types. (**c**) A summary of HeLa BAC lines generated in this report superposed over a phylogenetic representation of human kinesin and myosin motors annotated with standardized motor class and gene names, as adapted from refs 2,3. Genes normally expressed in HeLa cells are indicated with cyan (see Supplementary Table S1). For all combinations of N- and C-terminal tagging of human (h)- or mouse (m)-derived BACs, green indicates that a stably transfected HeLa BAC line is available (see Supplementary Table S2).

RESULTS

Microarray analysis of motor gene expression in cells

We wanted to determine which motors are expressed in HeLa cells, and how this expression pattern varies between different cell types. To address this challenge, we performed a single-platform transcription profiling analysis in HeLa cells, a human cell line used for high-throughput BAC transfection[14], and primary human immune cells before and after stimulation. We find that HeLa cells express more motor genes than either primary CD4+ T-lymphocytes or monocytes. *Ex vivo* T-cell activation increases the number of expressed motor genes to approximately that of HeLa cells, but we find fewer genes activated by monocyte differentiation (Fig. 1a and Supplementary Table S1). A comparison of HeLa cells to resting immunocytes identified a core set of 21 ubiquitously expressed human motors and another 32 expressed in at least one cell type (Fig. 1b and Supplementary Table S1). We enumerate the motor proteins endogenous to HeLa cells and highlight differences in motor gene expression between primary human cells.

Generating a motor BAC transgene and cell line collection

To generate a comprehensive transgene resource to study motor function in cells, C-terminal LAP or N-terminal NFLAP tags were introduced into all commercially available BAC transgenes encoding motor proteins to provide uniform tags for immunofluorescence microscopy (IFM), live-cell video microscopy and AP–MS (ref. 14). Murine and human genes were tagged as complementary gene sets with a nearly identical gene number for use as fluorescent transgenes or heterologous RNAi-resistance rescue factors[15,17], depending on the species origin of the cultured cell line, or to study motor function *in vivo* in mice. A BAC collection including 59 full-length human and 72 mouse motor genes was tagged by high-throughput recombination in *E. coli* (see Supplementary Table S2), transfected into HeLa cells and selected for stable incorporation of the transgene, as described previously[14]. The 86% overall success rate produced 227 cell lines (Fig. 1c) that we characterized by IFM and western blotting of cell lysates (see Supplementary Table S3). In most cases, the cells represent transformed pools, but we also prepared GFP-positive cell pools and clones by fluorescence-activated cell sorting (FACS) for genes of interest, (see Supplementary Table S3) and found levels of the recombinant human transgenes similar to the endogenous protein (see Supplementary Fig. S1), as previously noted for other BAC transgenes[15,20].

BAC transgene localization in cultured cells

We confirmed known mitotic localizations of motor proteins (see Supplementary Table S2) and performed an interphase localization

a

Localization	Genes
No signal	24
Cytoplasmic	10
Nuclear	12
Other	11

Localization	Genes	Motor protein
Centrosome	2	KIF2C, KIFC3
Actin-like	2	MYH9, MYH10
Cortex	5	KIF26A, MYO1B, MYO1C, MYO1G, MYO18A
Cell projections	1	KIF3C
Mitochondria	1	MYO19

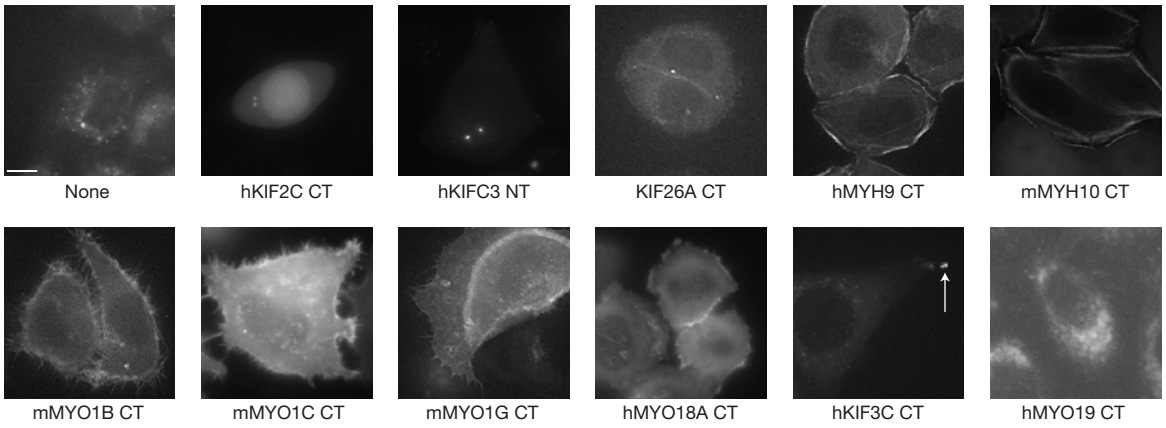

b

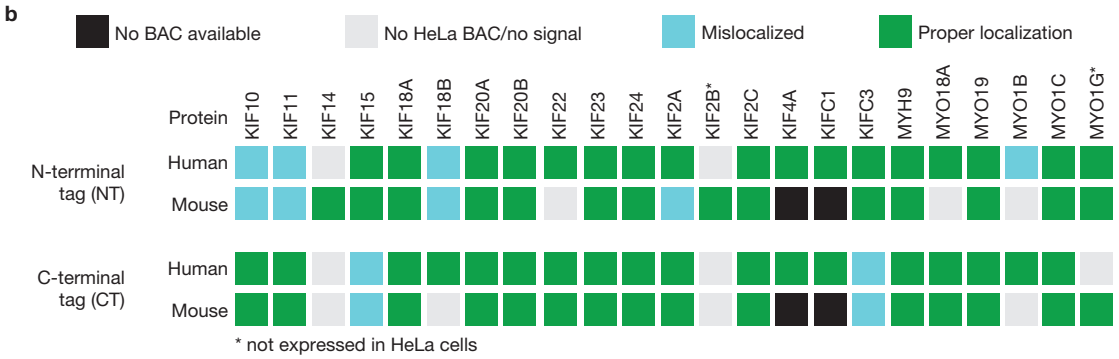

Figure 2 Localization of motor BAC transgenes in HeLa cells. (**a**) Top, summary of HeLa BAC transgene localization during interphase for 57 N- and C-terminally tagged motor genes into generic (left) and specific (right) categories; the latter motor proteins are named. Bottom, representative live-cell GFP fluorescence images are presented for untransfected HeLa cells (None) or expressing recombinant motor proteins tagged at their C (CT) or N terminus (NT), as indicated. Arrow indicates GFP staining at cell projection. Scale bar, 10 μm. (**b**) Localization summary for tagged motor proteins previously reported to have a non-cytoplasmic localization, as adapted from Supplementary Table S3. Squares indicate whether the BAC transgene was properly targeted (green), mislocalized (cyan), failed to generate a HeLa BAC line with detectable GFP (grey) or the BAC was not commercially available (black).

screen of all transgenic lines using IFM and time-lapse fluorescence microscopy. As predicted from previous work, many kinesin and myosin transgenes are targeted to recognizable interphase compartments that reflect a cellular function (Fig. 2a). We also observed that regulation of protein abundance through the cell cycle for human (see Supplementary Video S1) and mouse (see Supplementary Video S2) motor proteins was similar in HeLa cells, as expected from previous reports of cross-species BAC transgene function[13,15,17]. As we had generated both N- and C-terminally tagged human- and mouse-derived transgenes, this allowed us to compare the localization of transgenes tagged at different ends as an indirect functional readout. We found that 15 (67%) of 23 previously characterized kinesins and myosins localize properly as either the N- or C-terminally tagged recombinant motor protein. Another 6 motors are properly localized when tagged at only one end (Fig. 2b) regardless of whether the mouse- or human-derived gene was used. This illustrates that the choice of tagging site is important for function, as previously shown in yeast[22].

A subset of BACs was also transfected into mESCs to compare localization of the resulting protein with that observed in HeLa cells. IFM analysis in fixed cells revealed motor transgene localization to be broadly similar in HeLa cells and mESCs (see Supplementary Figs S2A,B and Table S3). Analysis of live cells with tagged Kinesin-2, a heterodimeric complex of KIF3A and KIF3C, also showed targeting to dynamic cell extensions, as expected[23], in HeLa cells (see Supplementary Fig. S2C and Supplementary Video S3) and mESCs (see Supplementary Video S4). Our analysis indicates which tagged motor BAC transgenes are properly localized in cells and may function across species.

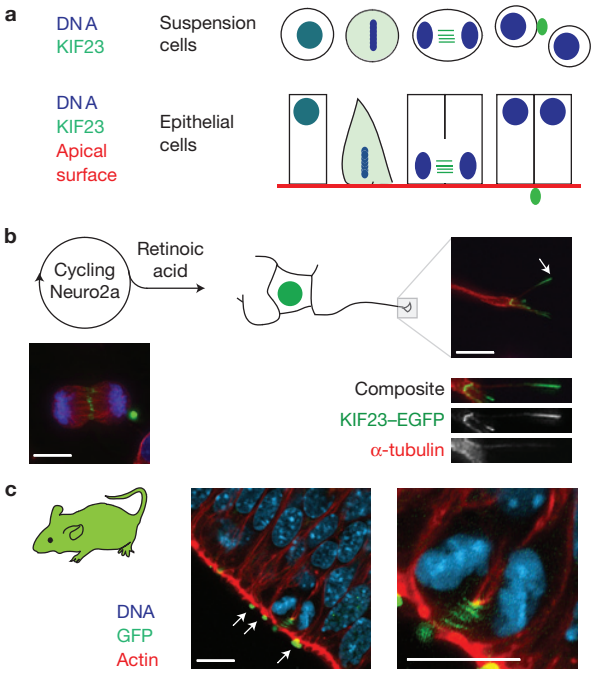

Figure 3 KIF23 localization in neuroblastoma and neural progenitor cells. (**a**) Idealized comparison of KIF23 localization (green) relative to DNA (blue) and the apical membrane (red) in suspension and polarized epithelial cells, as adapted from ref. 29. Schematic images, left to right, represent interphase, metaphase, anaphase (suspension cell, top) or cytokinesis (epithelial cell, bottom) and post-abscission. KIF23 is nuclear during interphase and cytoplasmic through early mitosis. From anaphase to cytokinesis it is concentrated at spindle midzone fibres, then midbodies. In epithelial cells, the cytokinesis proceeds from the basolateral to apical side and midbodies accumulate at the apical membrane. (**b**) Neuro2a cells fixed before (left) or after (right) differentiation with retinoic acid and stained for α-tubulin (red), GFP (green) and DNA (blue). In cycling Neuro2a cells, KIF23–EGFP is targeted to the spindle midzone and a residual midbody during cytokinesis. For Neuro2a cells differentiated with retinoic acid, an image of a representative neurite (arrow), and enlarged (2×) images (composite and individual GFP and α-tubulin channels) are shown. (**c**) Left, confocal section of the mouse embryonic neuroepithelium at embryonic day 14.5 (mid-neurogenesis) stained for DNA (blue) and filamentous actin (red) in KIF23–EGFP transgenic mice. Native GFP staining (green) shows multiple midbodies (arrows). Right, a magnified view of a cell undergoing cytokinesis with GFP staining midzone fibres between the basally-to-apically ingressing cleavage furrow and the apical surface of the cell. Scale bars, 10 μM.

KIF23 localization in multiple cell types

BACs include native regulatory information, often conserved across species[24], making them ideal for use in transgenic animals to characterize protein function *in vivo*. To illustrate this potential, we investigated the localization of recombinant human KIF23 in mouse cells and tissues. Of the kinesins required for cell division, some also have demonstrated interphase roles[25,26]. In human cells, KIF23 is required in the terminal stages of mitosis[27] and neurite outgrowth in post-mitotic neurons[28]. KIF23 labels the anaphase midzone and midbodies between cytokinesis and abscission (Fig. 3a and ref. 27), but its localization in neurites or native tissues is thus far undocumented by IFM.

In light of the published requirement for KIF23 in neurite outgrowth, we chose to investigate KIF23 localization in Neuro2a cells, a mouse neuroblastoma cell line that exits the cell cycle on treatment with retinoic acid to generate neurite processes. KIF23 was targeted to mitotic structures in untreated cells, as previously described, and identical to the pattern observed in HeLa cells and mESCs (ref. 29). In cells treated with retinoic acid, we found KIF23 targeted at the tips of cellular processes (Fig. 3b), consistent with a primarily mitotic motor localized in a functional interphase compartment.

To analyse KIF23 in tissues, we established a transgenic mouse line by pronuclear injection (see Supplementary Fig. S3a) and analysed a panel of tissues from the resulting animals by thin-section IFM. KIF23 was undetectable in representative non-proliferating tissues such as liver, kidney and absorptive intestinal epithelia (see Supplementary Figs S3B–D, respectively), suggesting that not all tissues have a post-mitotic role for KIF23. Bright midbodies, in contrast, decorated the epithelial surfaces of proliferative zones such as the embryonic brain (Fig. 3c) and intestinal crypt (see Supplementary Figs S3E,F). These same regions contained anaphase cells with spindle midzone staining (Fig. 3c and Supplementary Fig. S3G, respectively), showing that the *in vivo* distribution of KIF23 recapitulates previous work in cultured cells[29]. The absence of midbodies outside intestinal crypts (see Supplementary Fig. S3D) further indicates that midbodies persist in zones of cell proliferation and are lost as cells differentiate. Our results demonstrate that the same human-derived BAC transgene is readily portable to model cells and organisms.

Interaction screening for motor-specific binding proteins

Protein interaction analysis is a targeted approach to infer protein function but there are relatively few known motor binding proteins. Therefore, a central goal of this project was to prove the significance of motor BACs for systematic interaction analysis. To this end, 63 HeLa BAC pools were analysed by AP–MS.

To test the efficiency of recovering bait protein, clarified extracts from cycling and mitotically enriched cells were submitted for AP–MS. Overall, we recovered 61 (95%) of our transgenes from a total of 189 (87%) individual AP–MS experiments (see Supplementary Fig. S4A and Table S4). Label-free relative quantification of GFP-derived peptides (see Supplementary Fig. S4B) demonstrated a broad dynamic range for the recovery of motor transgenes from different samples (see Supplementary Fig. S4C), often successfully identifying proteins undetectable by western blotting.

AP–MS detected the expected transgene product in 189 samples, establishing a threshold for samples that can reveal interactions. Background subtraction against promiscuous binding proteins[30–32] identified 222 high-confidence interactions, including 45 (20%) that were previously characterized or had homologous interactions. Another 62 (28%) interactions are consistent with similar patterns of subcellular localization for the two proteins. Finally, genetic interactions support an extra 21 (10%) interactions (see Supplementary Table S5). The relatively small number of interactions and the high fraction (52%) supported by empirical data indicates that our background subtraction yielded high-confidence, high-affinity motor-selective interaction partners.

Combined localization and interaction studies have proved a powerful approach to investigate protein function[13,18]. Figure 4 superimposes localization data for 22 (39%) transgenes and all 178 interactors identified by AP–MS. The subset of 86 pairwise interactions that were previously reported, or validated by co-localization, are

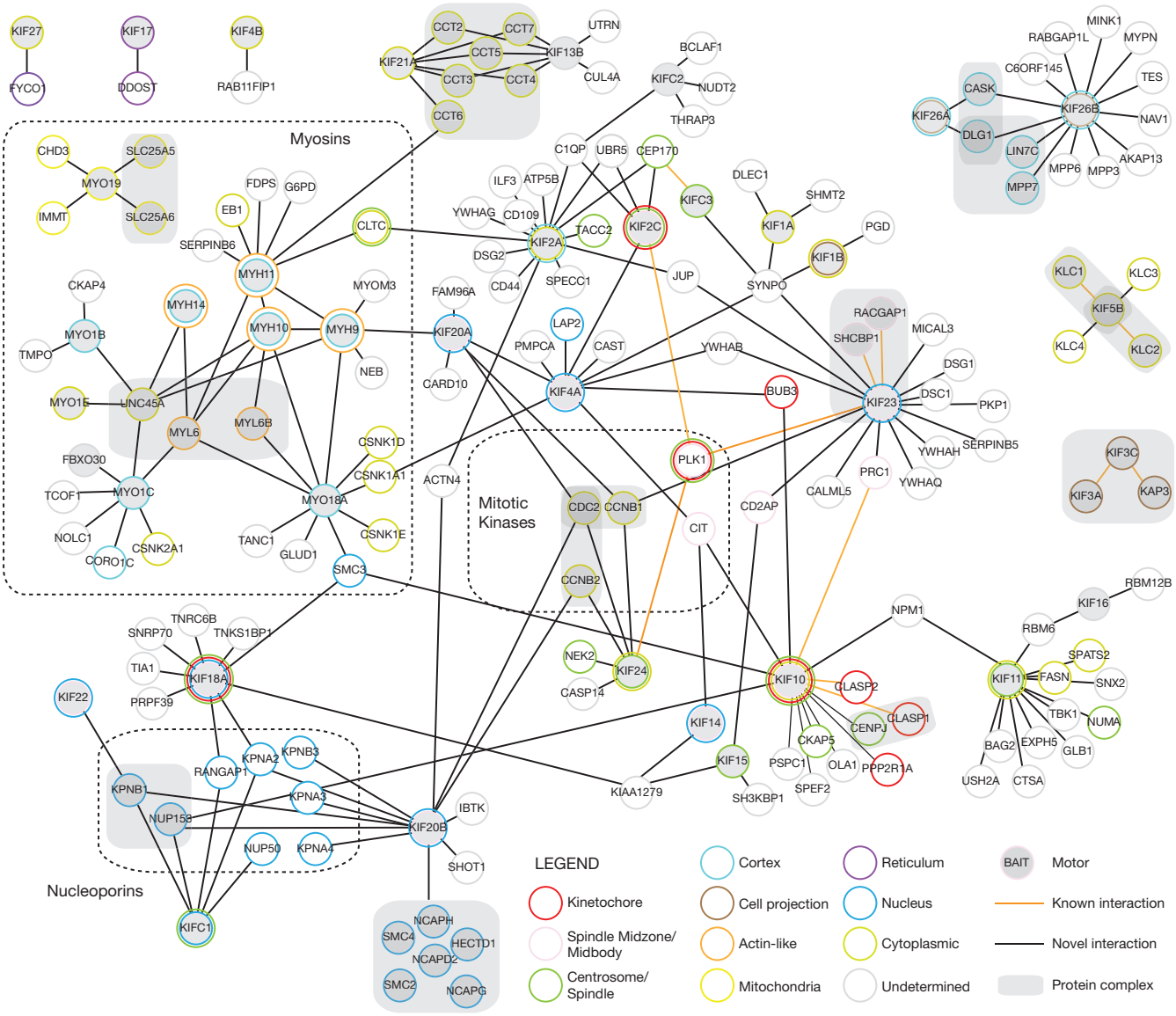

Figure 4 Composite localization–interaction data for the motor protein interactome. Summary of localization and interaction data for motor-selective interaction partners identified by AP–MS of myosin and kinesin BAC transgenes, adapted from Supplementary Table S5. Nodes representing proteins (shaded grey for motor proteins) and their subcellular localization (concentric coloured circles) are connected by edges that indicate previously reported (orange) or candidate (black) interactions. Annotated protein complexes are shaded (grey). Myosins, nucleoporins and mitotic kinases are indicated.

presented from three perspectives: interactions within a protein superfamily (motor proteins), interactions between two protein superfamilies (motors and protein kinases), and all other interactions that were previously reported or validated by co-localization.

In a screen of 56 motor proteins, we found 7 motor–motor interactions, none previously reported. This is consistent with each motor defining a unique subcellular compartment and supports an evolutionary argument for motor protein diversity. These interaction partners, including four reciprocal interactions, are all targeted to mitotic organelles (Fig. 5a).

Global and local protein phosphorylation is an important control mechanism for cellular processes. Therefore, we searched for interactions between motors and protein kinases. Among the 518 human protein kinases[33], 11 kinases and 3 accessory proteins bind 13 motors to define 25 protein–protein interactions. In 16 (64%) of the motor–kinase interactions, two mitotic proteins were linked. The interactions between KIF11 and TBK1 or KIF4A and casein kinase stand out because two primarily mitotic kinesins bind protein kinases with no clear link in mitosis. The remaining 7 pairwise interactions link non-mitotic proteins to candidate regulatory mechanisms (Fig. 5b).

Figure 5c illustrates localization–interaction maps for 27 previously reported and 16 candidate pairwise interactions, the latter dominated by regulatory light chains. For clarity, 13 interactions linking nuclear localized kinesins to nucleoporins are omitted.

Interaction screening of mitosis[13] or autophagy[34] proteins revealed networks consisting of linked multi-protein complexes that defined subnetworks functioning as protein machines. A survey of the entire motor interactome (Fig. 4) revealed only three such protein machines:

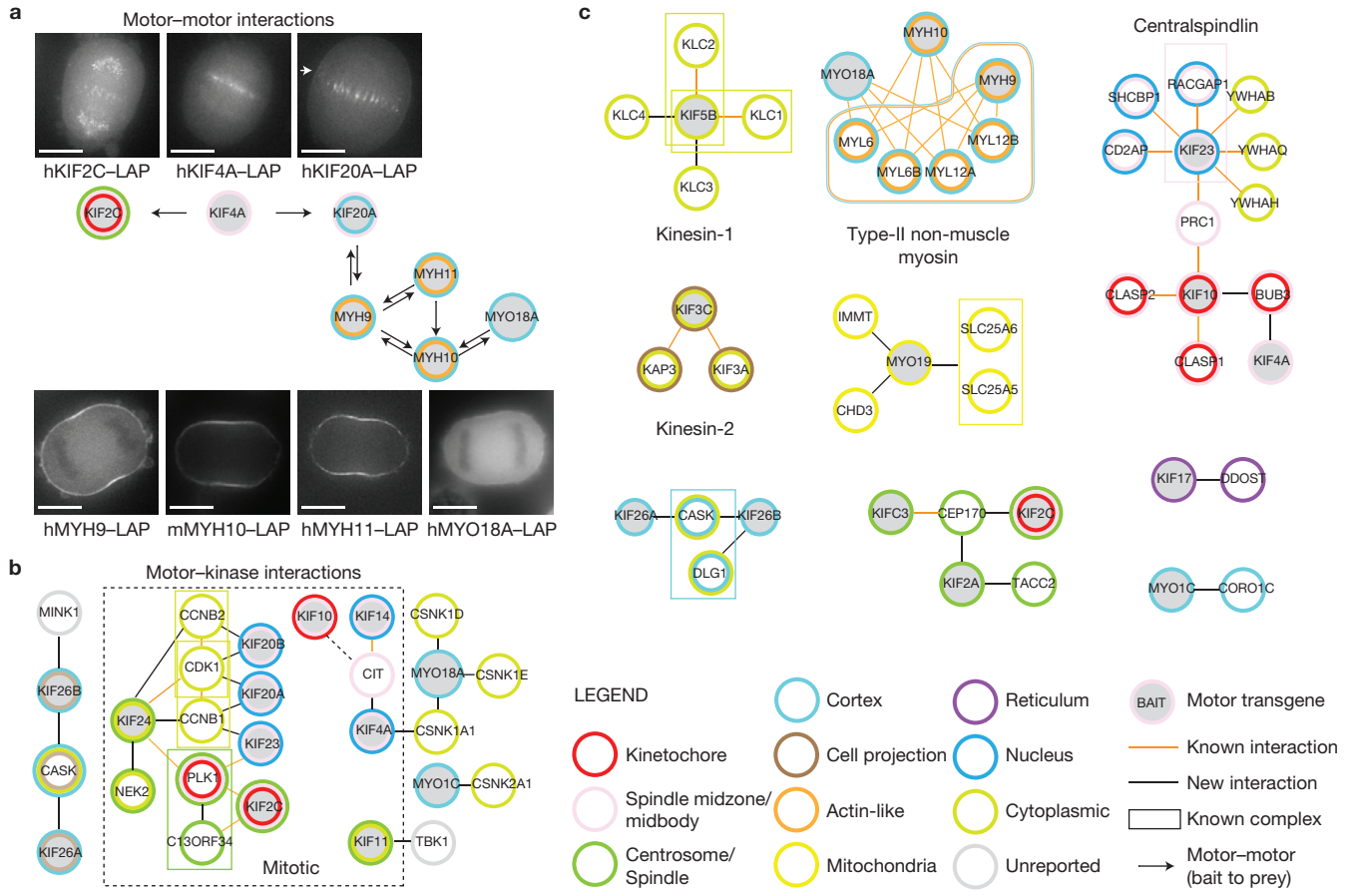

Figure 5 Summary of validated motor protein interaction partners. Localization–interaction summary for AP–MS screening hits previously validated by co-localization, physical or genetic interactions in the scientific literature, as adapted from Supplementary Table S5. (**a**) Summary of interactions between motor proteins discovered by AP–MS (centre); arrows point from transgene (bait) to interactor (prey). Surrounding the interaction map are GFP images of live cells in anaphase expressing BAC transgenes, as indicated. Cortical targeting of hKIF20A–LAP is indicated (arrow). Scale bars, 10 μm. (**b**) Localization–interaction summary for edges connecting motor proteins and protein kinases. Proteins required in cell division are inside the dashed square. (**c**) Combined localization–interaction map for the remaining validated interactions. Protein complexes are labelled with common names, if any, and coloured to indicate their subcellular localization.

the TCP-1 chaperone, cohesin and a densely linked myosin-associated network. Instead, motors bind light chains, protein kinases and nucleoporins. This observation suggests that motor proteins are most stably associated with regulatory factors, not their cognate organelles or cargoes.

A kinesin network modulates CEP170 targeting to centrosomes

The centrosome is the dominant microtubule-organizing centre in cells and is required for polarity, intracellular trafficking and accurate cell division. Although more than 300 centrosome-associated proteins have been identified[18,35], the function and regulation of many centrosome components remains an open question. We identified three centrosome-associated kinesins (KIF2A, KIF2C, KIFC3) that independently bind CEP170 (Fig. 5c and Supplementary Table S5), a PLK1-associated centrosomal protein with a role in microtubule organization[36]. In fixed cells, RNAi depletion of each kinesin or CEP170 caused no gross spindle defects, consistent with[37], aside from a small, but significant increase in metaphase spindle length (see Supplementary Fig. S5A). These results suggest that CEP170-associated proteins are important for metaphase spindle size control, but are not essential for spindle bipolarity.

Next, we investigated the role of these proteins in CEP170 targeting through the cell cycle using a HeLa BAC line as a reporter system (Fig. 6a). Qualitative analysis of fixed mitotic cells indicated that KIFC3, a known CEP170 binding partner[13], and KIF2C are individually required for proper CEP170 targeting to metaphase centrosomes (see Supplementary Fig. S5B). This result is consistent with the known dynamic interplay of mitotic centrosome components[18]; however, we also observed that KIF2A depletion enhanced the number of interphase cells with CEP170-positive centrosomes (Fig. 6b). To further investigate CEP170 dynamics, we used time-lapse fluorescence microscopy to improve the temporal resolution and quantification of CEP170 transgene fluorescence at centrosomes. Targeting of CEP170–LAP to centrosomes occurs in two waves, immediately before and after mitosis (see Supplementary Video S5). The first wave involves a gradual accumulation of CEP170 up to mitotic rounding, when most centrosome staining is lost. The second wave involves rapid targeting of CEP170 following cytokinesis that dissipates over hours. Targeting of known CEP170-binding proteins, either by treatment of cells with RNAi targeting KIFC3 (Fig. 6c,d) or a pharmacological inhibitor of PLK1 activity (see Supplementary Fig. S5C) markedly reduced the amount of CEP170

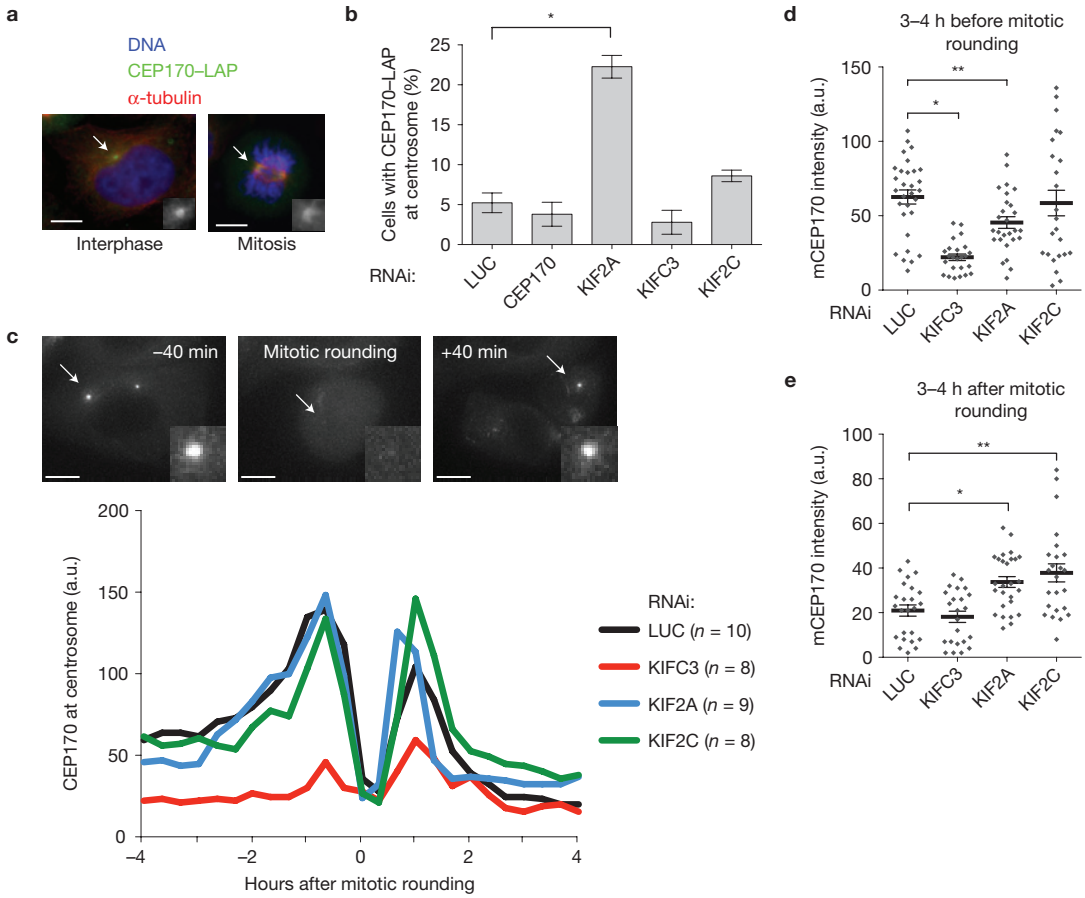

Figure 6 Three kinesins regulate CEP170 targeting to centrosomes. (**a**) A fixed HeLa BAC expressing mCEP170–LAP stained for DNA (blue), GFP (green) and α-tubulin (red). Insets contain enlarged GFP images of centrosomes (arrows). (**b**) The fraction of fixed, non-mitotic cells with GFP-positive centrosomes in clonal HeLa BAC line stably expressing mCEP170–LAP after treatment with RNAi targeting Luciferase (LUC, control), human CEP170, KIF2A, KIFC3 or KIF2C. Average of three experiments. Error bars, s.d.; $^{*}P < 10^{-4}$ ($n = 1{,}014$ cells) (Student's t-test). (**c**) Time-lapse imaging of the mCEP170–LAP HeLa cell clone after esiRNA depletion of interacting kinesin motors. Top, representative image projections of the mCEP170–LAP HeLa clonal line before (−40 min), during and after (+40 min) the onset of mitotic cell rounding. Insets present enlarged images of a representative centrosome (arrows) at each time point. Bottom, median integrated GFP intensity for mCEP170–LAP at centrosomes after treatment with esiRNA targeting Luciferase (LUC, $n = 10$ cells), KIFC3 ($n = 8$ cells), KIF2A ($n = 9$ cells) or KIF2C ($n = 8$ cells). (**d**) Statistical analysis of centrosomal GFP signal in cells treated with RNAi at three time points between 200–240 min, before mitotic rounding. Error bars, s.d. $^{*}P = 3 \times 10^{-9}$ ($n = 8$ cells); $^{**}P = 0.008$ ($n = 9$ cells) (Student's t-test). (**e**) Statistical analysis of centrosomal GFP signal in cells treated with RNAi at three time points between 200–240 min, after mitotic rounding. Error bars, s.d. $^{*}P = 0.0006$ ($n = 9$ cells); $^{**}P = 0.001$ ($n = 8$ cells) (Student's t-test). Scale bars, 10 μm.

at centrosomes in both targeting phases. A similar analysis of cells treated with KIF2A or KIF2C RNAi revealed persistent CEP170 staining after mitosis (Fig. 6d), consistent with the previously noted IFM phenotype of interphase cells depleted of KIF2A and a subtle effect of KIF2C depletion (Fig. 6b). Overall, quantitative imaging of CEP170 localization to centrosomes confirmed the functional significance of three pairwise protein interactions discovered by physical interaction screening.

Kinesin-1 forms asymmetric motor complexes

A central question in the study of intracellular trafficking is how a single motor protein sorts multiple cellular cargoes to their appropriate destination. The classic example is conventional kinesin, a complex of two KIF5B heavy chains and two kinesin light chains (KLCs) that regulate cargo binding and motor activity. KIF5B is a ubiquitously expressed microtubule plus-end-directed motor required to transport a variety of cargoes[10,12,34,38,39]. Mammalian genomes contain four KLC genes, each encoding multiple splice isoforms[40]. Biochemical analysis of tissue-derived conventional kinesin or engineered complementary DNA constructs for KLC1 and KLC2 in cultured cells suggests that KLC homodimers bind KIF5B exclusively[41,42]. However, it is unclear whether native KLCs uniquely form homodimers. We found that HeLa cells express all four KLC genes (see Supplementary Tables S1 and S5), permitting a re-evaluation of the KLC homodimer model by combining BAC transgenomics with the sensitivity of AP–MS.

First, we investigated whether the soluble KIF5B pool was different from that associated with membrane-bound organelles (MBOs). Light membranes were physically isolated from six different HeLa motor BAC lines for AP–MS using a simplified vesicle isolation protocol[43] to compare cytoplasmic and MBO-associated protein interactomes. KLC1, KLC2 and KLC4 were the only KIF5B–LAP-specific proteins identified among the vesicle markers recovered from captured MBOs. Moreover, quantification of MS peptide intensities revealed no difference in the stoichiometry of KLC1 or KLC2 between cytosolic and MBO-associated pools of conventional kinesin (Fig. 7a).

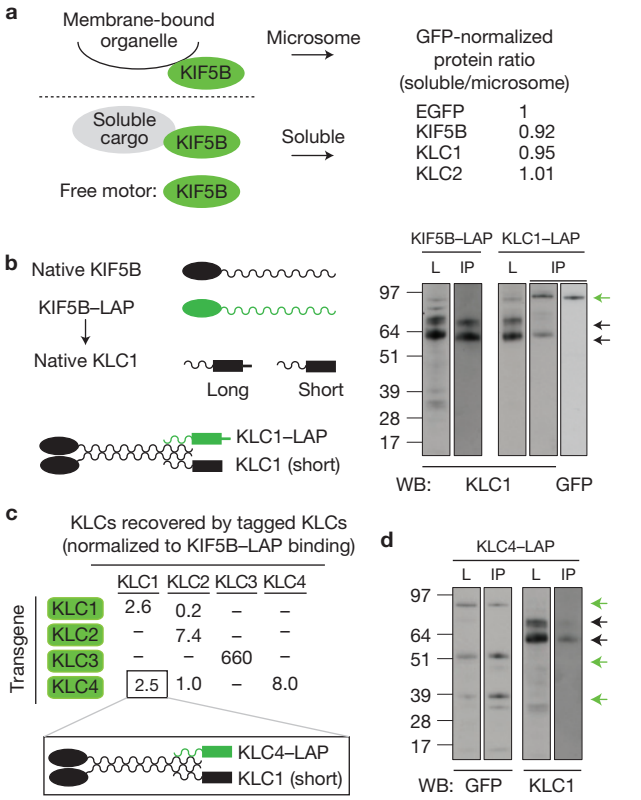

Figure 7 KIF5B binds KLC heterodimers in HeLa cells. (**a**) Quantification of KIF5B–LAP binding to KLCs in clarified lysate or microsomes purified from HeLa cells expressing KIF5B–LAP. The integrated signal intensity from KIF5B-, KLC1- and KLC2-derived peptides in each sample was normalized to EGFP-derived peptides as an internal control. (**b**) Left, a schematic summary of interaction data for native (black) KIF5B, KLC1 and their respective recombinant BAC transgene products (green). Right, anti-KLC1 and anti-GFP western blot (WB) analysis of lysates (L) and anti-GFP immune pellets (IP) from HeLa hKIF5B–LAP or hKLC1–LAP cells. The arrows mark the expected position of recombinant (green) and native KLC1 (black) isoforms. (**c**) Top, amount of each KLC protein recovered by systematic anti-GFP AP–MS of recombinant KLCs (green). The amount of each KLC recovered by recombinant KLCs is normalized to the amount of that KLC gene recovered by KIF5B–LAP. Bottom, a schematic illustration of KLC1 recovered by recombinant KLC4. (**d**) Western blot (WB) analysis of lysates (L) and anti-GFP immune pellets (IP) from HeLa hKLC4–LAP cells. The arrows mark the expected positions of recombinant KLC4 (green) and native KLC1 (black) isoforms. Uncropped images of blots are shown in Supplementary Fig. S7.

Therefore, we could not distinguish soluble from membrane-associated conventional kinesin.

Expression of multiple KLC genes and their isoforms may lead to combinatorial assembly of conventional kinesin containing KLC hetero and homodimers with distinct cargo-binding properties. To investigate this potential, we first generated clonal HeLa BAC lines for each KLC gene tagged at its 3′-most stop codon. LAP-tagged KLC1 and KLC3 transgenes were expressed as single isoforms, whereas KLC2 and KLC4 produced multiple polypeptides, consistent with predicted splice isoforms (see Supplementary Fig. S6A). As expected for functional KLCs, all four LAP-tagged transgenes bind native KIF5B (see Supplementary Fig. S6B) and KLC1–LAP, like KIF5B–LAP, binds native MBOs in HeLa cells (see Supplementary Fig. S6C).

Having established that KLC1–LAP binds KIF5B in HeLa cells, we further investigated which KLC1 isoform is recovered with KLC1–LAP. Western blotting of whole lysates and anti-GFP immune pellets revealed that whereas the KIF5B–LAP transgene binds all native KLC1 polypeptides, the KLC1–LAP transgene selectively binds a short isoform (Fig. 7b). Follow-up analysis of the AP–MS peptide coverage maps identified isoform-specific peptides to show that two native transcripts were recovered with KLC1–LAP (see Supplementary Fig. S6D), the longer splice product being barely undetectable by western blotting.

Systematic anti-GFP immunoprecipitation from KLC–LAP cell lines further supports the formation of asymmetric conventional kinesin in cells. Our AP–MS results indicated that KLC1–LAP and KLC4–LAP transgenes recover the products of other KLC genes (Fig. 7c and Supplementary Table S5) and independently confirmed binding of KLC4–LAP to KLC1 (Fig. 7d). Quantification of KLC recovered with each KLC transgene, relative to the equivalent KIF5B, further revealed promiscuity of KLC1 and KLC4, but not KLC2 and KLC3, transgenes. We note with interest that KLC3, the most divergent member of this protein family, does not recover other KLCs, and may form homodimers exclusively (Fig. 7c). Our biochemical analysis clearly demonstrates the formation of asymmetric conventional kinesin by some KLC gene products in HeLa cells.

DISCUSSION

A central challenge in systems biology is integrating data from single-gene analyses spanning multiple phenotypic assays, cell lines, model organisms, and investigators. Complementary starting points such as localization, physical or genetic interactions provide functional hypotheses to probe our understanding of physiologically relevant processes. Therefore, the development of standardized resources allowing proteomic analysis of gene function across cell lines and in the whole organism is essential for the future of systems biology. In this report we present a set of resources to investigate all members of a protein superfamily: the structurally related myosin and kinesin superfamily of cytoskeletal motors.

The use of recombinant BAC transgenes is a powerful, high-throughput approach to investigate motor protein function in multiple cell types as third alleles. In light of highly efficient BAC tagging (92%) and cell transfection (93%), the main limitation remains the availability of BACs containing the complete human gene (69%). The higher coverage for BACs containing orthologous mouse motor genes (87%) of similar size suggests that this will be remedied as more human-derived BAC libraries become available, with the possibility of BAC stitching to cover larger genes[44]. The generation of a transgenic mouse line expressing tagged KIF23 demonstrates that even essential genes can be studied *in vivo* using BAC transgenes.

Tandem-affinity tags are excellent tools to isolate stable protein complexes that are relatively clean of contaminating proteins[13]. However, recent work shows that with modern quantitative MS, nonspecific proteins can be filtered out even when a single anti-GFP step is performed to capture the tagged protein complexes[20]. Therefore, we adopted a more general approach relying on a large number of immunoprecipitation experiments with related genes and a universal tag to identify common nonspecific interactions. Our AP–MS analysis identified over 180 protein–protein interactions in HeLa cells. In combination with multiple cell treatments for each

cell line, we discovered an extra 10 interactors for 5 motors with previously known interaction partners[13]. The high proportion of known interactions (20%) or co-localization of binding partners (35%) indicates a high-quality interaction set. Motor–motor interactions were mitosis specific, consistent with assembly of supramolecular structures such as the spindle midzone or the actomyosin cortex. Interaction nodes binding multiple motor proteins can either regulate, such as PLK1 (ref. 45) and PRC1 (ref. 46), or be regulated by (Fig. 5b–d) their cognate binding partners. Mitotic protein complexes may be more soluble or stable, because transport motors (KIF5B and KIF3C) recovered known holoenzymes, but otherwise no cargo adaptors. Sucrose gradient analysis of conventional kinesin also indicates labile cargo binding (see Supplementary Fig. S7C). Overall, this study elaborates a set of protein interactions and validates the functionality of our BAC transgenes for use in appropriate cell lines.

The CEP170 localization network we describe illustrates how multiple motor proteins contribute to organelle assembly. Centrosome assembly involves organization of a complex protein mixture into a supramolecular structure, controlled by the cell cycle. Quantitative analysis of protein localization in live cells with BAC transgenes revealed changes in CEP170 targeting that were previously unclear using binary phenotypes or fixed time-point assays. The mechanism of CEP170 clearance by KIF2A and KIF2C reveals an active mechanism for post-mitotic centrosome remodelling. In this respect, CEP170 is a defined PCM marker whose epistatic relationship to other centrosome proteins can be investigated in greater detail.

An important discovery of this report is the formation of asymmetric conventional kinesin motor complexes in HeLa cells. This may contribute to motor regulation at the composite interaction surfaces formed by KLC heterodimers[38]. However, this potential does not extend across metazoans as many genomes encode only a single KLC gene. Therefore, combinatorial assembly of conventional kinesin may be a mammalian solution to the problem of cargo discrimination. Multiple KLC genes are expressed in primary human immune cells (see Supplementary Table S1), and presumably other cell types, suggesting that research on the consequences of asymmetry in light-chain composition could be an important topic to further understand the specificity of intracellular trafficking. □

METHODS

Methods and any associated references are available in the online version of the paper.

Note: Supplementary Information is available in the online version of the paper

ACKNOWLEDGEMENTS

Most of this project was funded by the European Commission through the Sixth Framework Programme Integrated Project MitoCheck (LSHG-CT-2004-503464). A.A.H. received support from the Max Planck Society and from Bundesministerium fuer Bildung und Forschung grants NGFN-2 SMP-RNAi (01GR0402) and NGFN-Plus (01GS0859). Y.T. was supported by a Postdoctoral Fellowship for Research Abroad from the Japan Society for the Promotion of Science. F.M-B. was supported by EMBO (ALTF 1080-2007). A.E. was a member of the International Max Planck Research School for Molecular Cell Biology and Bioengineering and a Technische Universität Dresden doctoral student. W.B.H. was supported by grants from the DFG (SFB 655, A2; TRR 83, Tp6) and the ERC (250197), by the DFG-funded Center for Regenerative Therapies Dresden, and by the Fonds der Chemischen Industrie. E.B. and E.G. were supported by the DFG Research Center and Cluster of Excellence—Center for Regenerative Therapies Dresden (FZ 111). We thank J. Jarrells and B. Schilling (MPI-CBG Microarray Facility) for processing microarray samples. M. Biesold, M. Augsburg, A. Ssykor, S. Bastidas and N. Berger provided assistance with cell culture and transfection. I. Nuesslein (MPI-CBG FACS Facility) performed FACS of transgenic HeLa pools. M. Theis and F. Buchholz helped produce esiRNAs. The Trangsgenic Core Facility and Biomedical Services at the MPI-CBG provided technical assistance in generating and maintaining the KIF23 transgenic mouse strain.

AUTHOR CONTRIBUTIONS

The project was conceived and the paper was written by Z.M. and A.A.H. E.G. and E.B. designed and executed immunology experiments. I.P. and Z.M. performed BAC tagging and generated BAC cell pools. I.I-B. performed IFM of BAC cells. F.M-B. and W.B.H. generated the KIF23–EGFP mouse strain. A.E. and F.M-B. performed IFM of tissues. M.J. and A.S. analysed all AP samples by MS and A.V. calculated peptide intensity scores. R.W.K. isolated vesicles from BAC cells. Y.T. characterized CEP170 interactions. Z.M. performed all other experiments.

COMPETING FINANCIAL INTERESTS

The authors declare no competing financial interests.

Published online at www.nature.com/doifinder/10.1038/ncb2689
Reprints and permissions information is available online at www.nature.com/reprints

1. Vale, R. D. & Milligan, R. A. The way things move: looking under the hood of molecular motor proteins. *Science* **288,** 88–95 (2000).
2. Miki, H., Okada, Y. & Hirokawa, N. Analysis of the kinesin superfamily: insights into structure and function. *Trends Cell Biol.* **15,** 467–476 (2005).
3. Berg, J. S., Powell, B. C. & Cheney, R. E. A millennial myosin census. *Mol. Biol. Cell* **12,** 780–794 (2001).
4. Hirokawa, N., Noda, Y., Tanaka, Y. & Niwa, S. Kinesin superfamily motor proteins and intracellular transport. *Nat. Rev. Mol. Cell Biol.* **10,** 682–696 (2009).
5. Hirokawa, N., Niwa, S. & Tanaka, Y. Molecular motors in neurons: transport mechanisms and roles in brain function, development, and disease. *Neuron* **68,** 610–638 (2010).
6. Ohsugi, M. *et al.* Kid-mediated chromosome compaction ensures proper nuclear envelope formation. *Cell* **132,** 771–782 (2008).
7. Zhu, C. *et al.* Functional analysis of human microtubule-based motor proteins, the kinesins and dyneins, in mitosis/cytokinesis using RNA interference. *Mol. Biol. Cell* **16,** 3187–3199 (2005).
8. Goshima, G. & Vale, R. D. The roles of microtubule-based motor proteins in mitosis: comprehensive RNAi analysis in the *Drosophila* S2 cell line. *J. Cell Biol.* **162,** 1003–1016 (2003).
9. Goshima, G. *et al.* Genes required for mitotic spindle assembly in *Drosophila* S2 cells. *Science* **316,** 417–421 (2007).
10. Semiz, S. *et al.* Conventional kinesin KIF5B mediates insulin-stimulated GLUT4 movements on microtubules. *EMBO J.* **22,** 2387–2399 (2003).
11. Patino-Lopez, G. *et al.* Myosin 1G is an abundant class I myosin in lymphocytes whose localization at the plasma membrane depends on its ancient divergent pleckstrin homology (PH) domain (Myo1PH). *J. Biol. Chem.* **285,** 8675–8686.
12. Verhey, K. J. *et al.* Cargo of kinesin identified as JIP scaffolding proteins and associated signalling molecules. *J. Cell Biol.* **152,** 959–970 (2001).
13. Hutchins, J. R. *et al.* Systematic analysis of human protein complexes identifies chromosome segregation proteins. *Science* **328,** 593–599 (2010).
14. Poser, I. *et al.* BAC TransgeneOmics: a high-throughput method for exploration of protein function in mammals. *Nat. Methods* **5,** 409–415 (2008).
15. Bird, A. W. & Hyman, A. A. Building a spindle of the correct length in human cells requires the interaction between TPX2 and Aurora A. *J. Cell Biol.* **182,** 289–300 (2008).
16. Bird, A. W. E. *et al.* High-efficiency counterselection recombineering for site-directed mutagenesis in bacterial artificial chromosomes. *Nat. Methods* **9,** 103–109 (2011).
17. Kittler, R. *et al.* RNA interference rescue by bacterial artificial chromosome transgenesis in mammalian tissue culture cells. *Proc. Natl Acad. Sci. USA* **102,** 2396–2401 (2005).
18. Jakobsen, L. *et al.* Novel asymmetrically localizing components of human centrosomes identified by complementary proteomics methods. *EMBO J.* **30,** 1520–1535 (2011).
19. Vermeulen, M. *et al.* Quantitative interaction proteomics and genome-wide profiling of epigenetic histone marks and their readers. *Cell* **142,** 967–980 (2010).
20. Hubner, N. C. *et al.* Quantitative proteomics combined with BAC TransgeneOmics reveals *in vivo* protein interactions. *J. Cell Biol.* **189,** 739–754 (2010).
21. Anko, M. L., Morales, L., Henry, I., Beyer, A. & Neugebauer, K. M. Global analysis reveals SRp20- and SRp75-specific mRNPs in cycling and neural cells. *Nat. Struct. Mol. Biol.* **17,** 962–970 (2010).
22. Huh, W. K. *et al.* Global analysis of protein localization in budding yeast. *Nature* **425,** 686–691 (2003).
23. Jimbo, T. *et al.* Identification of a link between the tumour suppressor APC and the kinesin superfamily. *Nat. Cell Biol.* **4,** 323–327 (2002).

24. Levy, S., Hannenhalli, S. & Workman, C. Enrichment of regulatory signals in conserved non-coding genomic sequence. *Bioinformatics* **17,** 871–877 (2001).
25. Midorikawa, R., Takei, Y. & Hirokawa, N. KIF4 motor regulates activity-dependent neuronal survival by suppressing PARP-1 enzymatic activity. *Cell* **125,** 371–383 (2006).
26. Jones, W. M., Chao, A. T., Zavortink, M., Saint, R. & Bejsovec, A. Cytokinesis proteins Tum and Pav have a nuclear role in Wnt regulation. *J. Cell Sci.* **123,** 2179–2189.
27. Steigemann, P. *et al.* Aurora B-mediated abscission checkpoint protects against tetraploidization. *Cell* **136,** 473–484 (2009).
28. Yu, W., Sharp, D. J., Kuriyama, R., Mallik, P. & Baas, P. W. Inhibition of a mitotic motor compromises the formation of dendrite-like processes from neuroblastoma cells. *J. Cell Biol.* **136,** 659–668 (1997).
29. Ettinger, A. W. *et al.* Proliferating versus differentiating stem and cancer cells exhibit distinct midbody-release behaviour. *Nat. Commun.* **2,** 503 (2011).
30. Theis, M. *et al.* Comparative profiling identifies C13orf3 as a component of the Ska complex required for mammalian cell division. *EMBO J.* **28,** 1453–1465 (2009).
31. Matos, J. *et al.* Dbf4-dependent CDC7 kinase links DNA replication to the segregation of homologous chromosomes in meiosis I. *Cell* **135,** 662–678 (2008).
32. Maffini, S. *et al.* Motor-independent targeting of CLASPs to kinetochores by CENP-E promotes microtubule turnover and poleward flux. *Curr. Biol.* **19,** 1566–1572 (2009).
33. Manning, G., Whyte, D. B., Martinez, R., Hunter, T. & Sudarsanam, S. The protein kinase complement of the human genome. *Science* **298,** 1912–1934 (2002).
34. Behrends, C., Sowa, M. E., Gygi, S. P. & Harper, J. W. Network organization of the human autophagy system. *Nature* **466,** 68–76 (2010).
35. Nogales-Cadenas, R., Abascal, F., Diez-Perez, J., Carazo, J. M. & Pascual-Montano, A. CentrosomeDB: a human centrosomal proteins database. *Nucl. Acids Res.* **37,** D175–D180 (2009).
36. Guarguaglini, G. *et al.* The forkhead-associated domain protein Cep170 interacts with Polo-like kinase 1 and serves as a marker for mature centrioles. *Mol. Biol. Cell* **16,** 1095–1107 (2005).
37. Tanenbaum, M. E. *et al.* Kif15 cooperates with eg5 to promote bipolar spindle assembly. *Curr. Biol.* **19,** 1703–1711 (2009).
38. Hammond, J. W., Griffin, K., Jih, G. T., Stuckey, J. & Verhey, K. J. Co-operative versus independent transport of different cargoes by Kinesin-1. *Traffic* **9,** 725–741 (2008).
39. Cox, R. T. & Spradling, A. C. Milton controls the early acquisition of mitochondria by *Drosophila* oocytes. *Development* **133,** 3371–3377 (2006).
40. Gyoeva, F. K., Bybikova, E. M. & Minin, A. A. An isoform of kinesin light chain specific for the Golgi complex. *J. Cell Sci.* **113,** 2047–2054 (2000).
41. DeBoer, S. R. *et al.* Conventional kinesin holoenzymes are composed of heavy and light chain homodimers. *Biochemistry* **47,** 4535–4543 (2008).
42. Gyoeva, F. K., Sarkisov, D. V., Khodjakov, A. L. & Minin, A. A. The tetrameric molecule of conventional kinesin contains identical light chains. *Biochemistry* **43,** 13525–13531 (2004).
43. Klemm, R. W. *et al.* Segregation of sphingolipids and sterols during formation of secretory vesicles at the trans-Golgi network. *J. Cell Biol.* **185,** 601–612 (2009).
44. Kotzamanis, G. & Huxley, C. Recombining overlapping BACs into a single larger BAC. *BMC Biotechnol.* **4,** 1 (2004).
45. Liu, X., Zhou, T., Kuriyama, R. & Erikson, R. L. Molecular interactions of Polo-like-kinase 1 with the mitotic kinesin-like protein CHO1/MKLP-1. *J. Cell Sci.* **117,** 3233–3246 (2004).
46. Mollinari, C. *et al.* Ablation of PRC1 by small interfering RNA demonstrates that cytokinetic abscission requires a central spindle bundle in mammalian cells, whereas completion of furrowing does not. *Mol. Biol. Cell* **16,** 1043–1055 (2005).

METHODS

Cell culture and imaging. HeLa cells and mouse R1 embryonic stem cells[47] (mESCs) stably expressing tagged BACs were established and cultured as described previously[14]. Mouse Neuro2a (ref. 48) neuroblastoma cell culture, transfection and selection were identical to HeLa cells. BI2536 (Calbiochem, 100 nM), thymidine (Sigma-Aldrich, 2 mM), *S*-trityl-L-cysteine (Sigma-Aldrich, 2 μM) or nocodazole (Sigma-Aldrich, 250 ng ml^{-1}) were added to the imaging medium, as required.

Gene-specific PCR flanking the tagging site was used to confirm the identity and proper tagging of each BAC, as described previously[14]. Anti-GFP western blotting of lysate for each HeLa BAC pool was performed on nitrocellulose membranes (GE Healthcare) using mouse-anti-GFP clone 7.1 (Roche Applied Sciences, catalogue number 11814460001, 0.2 μg ml^{-1}), goat-anti-mouse HRP conjugate (Jackson ImmunoResearch) antibodies and the ECL Plus detection system (GE Healthcare). Of 230 HeLa BAC pools, 116 (51%) had no detectable GFP signal, and 79 (33%) showed the GFP-positive band of expected size. The 32 (14%) BAC pools expressing truncated proteins included 28 tagged, heterologously expressed motors and 4 tagged, endogenously expressed motors (see Supplementary Table S3). Therefore, we expect that BACs encoding endogenous motors produce the correct gene product.

The frequency of GFP-positive cells in HeLa BAC pools was generally higher than 10%. Expression of recombinant protein varies between FACS-sorted HeLa BAC clones (see Supplementary Fig. S1), as previously reported[15]. When multiple bands appear in western blots of HeLa BAC pool lysates, those bands are also observed in FACS-sorted clones (see Supplementary Fig. S6A).

To image HeLa and mESC BAC lines, cells were grown overnight on 11-mm glass coverslips for paraformaldehyde (PFA) or cold methanol fixation and staining, as described previously[13]. Primary antibodies included polyclonal goat-anti-GFP (prepared by the MPI-CBG Protein Expression Facility, 1 μg ml^{-1}), mouse anti-α-tubulin (Sigma-Aldrich, clone DM1A, 0.5 μg ml^{-1}) and rabbit anti-APC (Abcam, ab15270, 1:2,000). Secondary staining included Alexa-conjugated antibodies (Invitrogen, catalogue numbers A21203 and A31573, 1 μg ml^{-1}) as required, and Hoechst 33342 (Calbiochem, 10 μg ml^{-1}) before mounting coverslips with Mowiol (Calbiochem). Images were taken on a wide-field microscope (Axioplan 2; Zeiss) equipped with a CS4742-95 CCD (charge-coupled device) camera (Hamamatsu GmbH) and processed using Photoshop (Adobe).

For live-cell fluorescence imaging, cells were grown in 8-well Lab-Tek II imaging chambers (Nunc GmbH). Standard culture medium was exchanged for CO_2-independent medium (Invitrogen) before imaging on a DeltaVision (Applied Precision) instrument equipped with a CoolSnap HQ CCD camera (Princeton Instruments) controlled by softWoRx software (Applied Precision) in a climate-controlled environment maintained at 37 °C.

Transgenic Neuro2a cells were seeded overnight on 11 mm coverslips in 24-well plates, differentiated, fixed, stained, as previously described[29], and imaged on a DeltaVision system.

We confirmed the phenotypic effects for mitotic enrichment protocols by imaging live HeLa cells expressing mCherry–Histone 2B and TUBB1–LAP (ref. 13; see Supplementary Fig. S4A). HeLa cells were 0.5–1% mitotic in medium alone and 20–30% mitotic following double thymidine synchronization and release[49] (10–12 h). Prometaphase arrest using nocodazole[13] (18 h) or *S*-trityl-L-cysteine (18 h; ref. 50) resulted in 50–70% rounded cells with the expected microtubule phenotypes.

Endoribonuclease-prepared short interfering RNAs (esiRNAs) were prepared using the following primers (see Supplementary Table S6), as described previously[51]. Reverse-transfection with Oligofectamine (Invitrogen) was performed according to the manufacturer's protocol with the modifications outlined below. For IFM, HeLa cells were reverse-transfected with 0.35 μg esiRNA and 1.5 μl Oligofectamine in 24-well tissue culture dishes containing a glass coverslip in each well at a density of 40,000 cells per well. For live-cell imaging, a clonal (mouse CEP170–LAP) HeLa cell line was reverse-transfected with 0.3 μg esiRNA and 1 μl Oligofectamine in 8-well Lab-Tek II (Nunc GmbH) or μ-Slide 8-well (Ibidi GmbH) imaging chambers. Two days after transfection, we exchanged the medium and began live-cell imaging, as described above. Contrary to the phenotype reported for U2OS cells[52], but broadly consistent with a recent publication[37], we observed no monopolar spindles in KIF2A-depleted HeLa cells.

Fetal calf serum (FCS) and human serum (HS) used for immunocyte culture were heat-inactivated and filtered before use. Human peripheral blood mononuclear cells (PBMCs) were isolated from the buffy coats of anonymous blood donors (Red Cross blood donation service in Dresden) by Ficoll density gradient centrifugation and resuspended in RPMI (Invitrogen). Immune cell types were isolated with MACS MicroBeads (Miltenyi Biotec), cultured and collected for flow cytometry or total RNA isolation. To prepare flow cytometry samples, 1×10^5 cells were incubated for 30 min at 4 °C with fluorescently conjugated antibodies (BD Bioscience, 1.4 μg ml^{-1} unless otherwise indicated), washed and resuspended in 1 ml FACS buffer (1% BSA and 0.1% sodium azide in PBS) and analysed within 24 h on a BDLSRII Flow Cytometer System operated by FACS Diva (BD Biosciences) software. Raw flow cytometry data were analysed using FlowJo version 7.5 (Tree Star). All cell types were >95% pure.

Monocytes were isolated from PBMCs using MACS CD14 microbeads, seeded at a density of 2.5×10^6 cells per well in 6-well dishes and differentiated, as described below. Macrophages were generated by culturing monocytes in DMEM GlutaMAX (Invtirogen) supplemented with L-glutamine, penicillin/streptomycin, 20% FCS and 10% HS. Medium was replaced at days 1 and 5. Cells were collected after 7 days. For flow cytometry, macrophages were stained with CD14–FITC (clone M5E2, catalogue number 555397), CD16–PB (clone 3G8, catalogue number 558122, 0.8 μg ml^{-1}), CD45RO–PeCy7 (clone UCHL1, catalogue number 337168), CD31–PE (clone WM59, catalogue number 555446), CD25–APC–Cy7 (clone M-A251, catalogue number 557753) and CD69–APC (clone L78, catalogue number 340560).

Immature dendritic cells were obtained by culturing monocytes for six days in RPMI supplemented with 3% FCS, L-glutamine, penicillin/streptomycin, 50 ng ml^{-1} GM-CSF (R&D Systems) and 10 ng ml^{-1} IL-4 (R&D Systems). This medium was exchanged for RPMI supplemented with 5% FCS, L-glutamine, 10 ng ml^{-1} lipopolysaccharide and 100 U ml^{-1} interferon gamma (R&D Systems) and incubated for 24 h to prepare the mature dendritic cells. For flow cytometry, dendritic cells were stained with CD14–PeCy7 (clone M5E2, catalogue number 557742), CD40–APC (clone 5C3, catalogue number 555591), CD45RA–PE (clone HI100, catalogue number 555489) and CD1a–FITC (clone HI149, catalogue number 555806).

CD4+ T-cells were isolated using a primary negative depletion of PBMCs using MACS Naïve CD4+ T Cell Isolation Kit II or Memory CD4+ T Cell Isolation Kit II, followed by secondary negative depletion with CD25 microbeads (Miltenyi Biotec) to remove regulatory T-cells. The resulting naive or memory T-cells were resuspended in X-Vivo (Lonza) medium supplemented with 10% HS, seeded at 200,000 cells per well in 96-well plates (Corning V-plates) and stimulated with a Dynabeads CD3/CD28 T-cell expander (Invitrogen) for 3 days. For flow cytometry, T-cells were stained with CD3–APC (clone UCHT1, catalogue number 555335), CD4–PB (clone RPA-T4, catalogue number 558116, 0.8 μg ml^{-1}), CD8–PerCP (clone SK1, catalogue number 345774), CD45RO–PeCy7, CD25–APC–Cy7, CD40L–PE (clone 89-76, catalogue number 340477) and CD69–FITC (clone FN50, catalogue number 557049).

KIF23–EGFP transgenic mouse analysis. Transgenic mice were prepared by pronuclear injection of purified BAC DNA into C57BL/6 oocytes. Tail clippings from the resulting mice were genotyped using the C-terminal checking primers. For microscopy, adult mice and embryos were selected for tissue isolation. Midbody fluorescence signal in embryos was inherited from either male or female transgenic parents. A female mouse aged 32 weeks was euthanized to prepare tissue lysates for anti-GFP western blot analysis.

Mouse brains from embryonic day 14.5 embryos or tissues from adult mice were fixed overnight at 4 °C with 4% PFA in 120 mM phosphate buffer, at pH 7.4. The fixed samples were embedded (4% agarose in PBS) and sectioned (50 μm) with a Vibratome (Leica Microsystems). Sections were permeabilized (0.3% Triton X-100 in PBS, 30 min), quenched (100 mM glycine, 30 min), blocked (10 min) in antibody dilution buffer (PBS, 300 mM NaCl, 0.2% gelatin), stained (DAPI and phalloidin, 1 h) and mounted in Mowiol. Images were acquired on a Zeiss LSM 510 Meta, using a ×63 Plan-Apochromat 1.4 NA oil-immersion objective (Carl Zeiss).

Microarray transcription profiling. Total RNA was isolated from cell pellets using Trizol (Invitrogen) following the manufacturer's protocol. Immune-cell-derived samples were analysed as biological triplicates. HeLa cell samples, parental HeLa cells and 13 HeLa BAC pools or clones were analysed as singles. The MPI-CBG microarray facility performed all RNA labelling, hybridization and microarray scanning following the Agilent One-Colour Microarray-Based Gene Expression Analysis (Quick Amp) protocol version 5.7. Briefly, 1.65 μg of Cy3-labelled complementary RNA was hybridized to human whole transcriptome microarrays (Agilent, 4x44K, AMADID: 014850) and scanned using the Agilent Microarray Scanner (Agilent). Agilent kinesin or myosin (134 microarray probes) and all KLC (8 probes) genes. Raw image data were converted into numerical data using Agilent Feature Extraction Software, version 10.1. Quantile normalization of data in two batches (HeLa or immune cell samples) was performed with Partek Genomics Suite 6.5 (Partek). Comparison of microarray probe intensities to the published deep sequencing and proteome in HeLa cells[53] established 68 (48%) true positive and 28 (20%) true negative probes. For the remaining 21 (34%) probes, 18 were confirmed as true positives or true negatives on the basis of immunocyte-selective expression profiles in BioGPS (ref. 54), the Gene Expression Omnibus[55] (GEO) and the scientific literature (see Supplementary Table S1).

DOI: 10.1038/ncb2689

Biochemical methods. For AP–MS samples, HeLa BAC pools were cultured to 50% confluent monolayers before treatment, collected, immunoprecipitated with polyclonal goat anti-GFP crosslinked to Sepharose protein G (GE Healthcare) and finally eluted with low-pH glycine, as described previously[56]. Eluate was immediately neutralized with 1 M Tris–HCl (pH 9.0) and submitted for trypsin digestion (90%), as below, or quality control (10%) by western blotting and silver staining.

A protocol for subcellular-fractionation- and immuno-adsorbent based isolation of vesicular membranes[43] was adapted for recovery of motor-protein-associated vesicles from HeLa cells at 4 °C. The immuno-isolation matrix was prepared by conjugation of polyclonal goat anti-GFP antibodies with diazocellulose[57] and stored at 4 °C in PBS-G (PBS with 0.1% gelatin (EMD)). Approximately 10^8 cells from each HeLa BAC pool were collected by scraping into MB (50 mM HEPES–KOH (pH 7.4), 150 mM NaCl, 2 mM $MgCl_2$, 1 mM EGTA and 10% sucrose) and physically disrupted by passing through a narrow-gauge needle. Lysates were clarified by centrifugation (10 min, 10,000*g*) and vesicles were isolated by pelleting the supernatant (90 min, 180,000*g*) onto a 50 µl 35% (w/w) sucrose cushion. The cushion and membrane-rich interface were resuspended in a total volume of 500 µl with PBS-G and gently clarified (5 min, 1,000*g*). The supernatant was incubated with the anti-GFP matrix (4 °C, 4 h) on a rotating shaker. The matrix was recovered by centrifugation (2 min, 1,500*g*), rinsed 3 times and resuspended in PBS-G. The resulting material was split evenly between two elution protocols before neutralizing with Tris–HCl, as above; specific elution (overnight, 4 °C) with TEV protease (MPI-CBG Protein Expression Facility), or low-pH glycine[56].

To prepare microsomes for density gradient centrifugation, HeLa cells were collected by scraping in MB, physically disrupted and clarified, as above. Microsomes were pelleted (90 min, 100,000*g*), resuspended in MB and mixed with an equal volume of iodixanol (GE Healthcare). A step-wise 20–5% iodixanol density gradient in MB was layered over the resuspended microsomes for centrifugation (4 h, 100,000*g*). Density gradient fractions were resolved by denaturing PAGE and analysed by western blotting.

Direct analysis of protein complexes by mass spectrometry. Neutralized protein samples were digested overnight with 16 ng µl^{-1} trypsin (Promega) at 39 °C. The tryptic peptides were captured using a UltraMicroSpin-C18 (The Nest Group) cartridge and eluted with 4:1 acetonitrile(ACN)/water buffered with 0.1% trifluoroacetic acid (TFA), dried and dissolved in 10 µl 0.1% TFA. Of the resulting sample, 40% was loaded onto a Ultimate 3000 nanoLC system (Dionex), concentrated on a trapping microcolumn (5 mm × 300 mm i.d.) packed with 5 µm C18 PepMAP100 (Dionex) and resolved using a nanocolumn (15 cm × 75 µm i.d.) packed with 3 µm C18 PepMAP100 (Dionex) operating a 3 h elution gradient of solvent A (95:5 H_2O/ACN (v/v), 0.1% formic acid) and solvent B (20:80 H_2O/ACN (v/v), 0.1% formic acid), as follows: 73 min (5–20% B), 72 min (20–50% B), 5 min (50–100% B), 10 min (100% B), 10 min (100–5% B) and 10 min (5% B). The nanoLC interfaced on-line with an LTQ Orbitrap hybrid mass spectrometer (Thermo Fisher Scientific) through a robotic nanoflow ion source TriVersa (Advion BioSciences) equipped with a liquid chromatography coupler and a 4.2 µm nozzle diameter nanoESI chip operated at 1.7 kV ionization voltage. Chipsoft 6.4 (Advion Biosciences) monitored electrospray current stability. One cycle of data-dependent acquisition mode MS/MS, under the control of Xcalibur 2.0 (Thermo Fisher Scientific), consisted of one survey microscan (m/z = 300–1600, target mass resolution = 60,000 full-width at half-maximum, target value = 10^6 ions) in the Orbitrap analyser and then fragmentation of the four most abundant multiply charged precursors was acquired in one microscan (normalized collision energy = 35%, linear ion trap target value = 10^4 ions, ion selection threshold = 400 counts, precursor ions isolation width = 2 a.m.u.). Activation parameters (q = 0.25, activation time = 30 ms and dynamic exclusion = 90 s) were applied. The .raw files were converted to .mgf (MASCOT generic format) format using the extract_msn utility in Bioworks 3.1 (Thermo Fisher Scientific) and searched against the International Protein Index—Human database (68360 sequence entries) using MASCOT v. 2.4 (Matrix Science). In the ESI-Trap instrument profile, precursor and fragment mass tolerances were 10 ppm and 0.6 Da, respectively. One missed cleavage, methionine oxidation, N-terminal acetylation and phosphorylations (serine, threonine and tyrosine) were allowed. MASCOT protein identifications had a total score above 60 considering individual peptides with ion scores above 20.

The .raw files were first converted to mzXML format using ReAdW v 4.3.1 (ref. 58). MASCOT data files were separately processed through the TransProteomic Pipeline[59] to generate a pep.xml file compatible with label-free quantification by SuperHirn v0.03 (ref. 60). Default settings were used with the following exceptions: MS1 retention time tolerance = 2, MS2 PPM m/z tolerance = 15, MS1 feature CHRG range min = 2, MS1 data centroid data = 0, MS1 feature signal to noise threshold = 3.0. Each mzXML and its corresponding pep.xml peptide identification file were individually processed using SuperHirn feature extraction and master map creation tools to calculate the integrated peptide intensity for each identified peptide in each MS acquisition.

Unique peptides were mapped onto the recombinant tag and expected motor protein sequence. Candidate interaction partners were identified on the basis of the number of unique gene-specific peptides in the sample and their cumulative MASCOT score. We discarded candidate interactors appearing in control lines (HeLa–GFP or HeLa) or when the expected transgene was not detected, as previously described[30–32]. Finally, we discarded candidate interactors binding more than five motor proteins. The resulting pairwise interaction list was compared to protein–protein interactions in BioGRID (2011 version)[61], co-localization data and the scientific literature (see Supplementary Table S5).

Data accession. Raw microarray data for HeLa cells (GSE33271), T-cell (GSE33272) and monocyte-lineage (GSE33273) RNA are available at the GEO (ref. 55). Representative HeLa BAC images can be viewed online at The Cell: an Image Library (http://www.cellimagelibrary.org, project ID: P20234). Individual microarray and image files are annotated (see Supplementary Tables S7 and S8).

Resource access. Send requests for individual *E. coli* stocks containing modified BAC transgenes (see Supplementary Table S2), transgenic HeLa cell and mESC lines (see Supplementary Table S3) to I. Poser (poser@mpi-cbg.de). Unmodified BACs are commercially available (BACPac Resources).

47. Nagy, A., Rossant, J., Nagy, R., Abramow-Newerly, W. & Roder, J. C. Derivation of completely cell culture-derived mice from early-passage embryonic stem cells. *Proc. Natl Acad. Sci. USA* **90,** 8424–8428 (1993).
48. Olmsted, J. B., Carlson, K., Klebe, R., Ruddle, F. & Rosenbaum, J. Isolation of microtubule protein from cultured mouse neuroblastoma cells. *Proc. Natl Acad. Sci. USA* **65,** 129–136 (1970).
49. Whitfield, M. L. *et al.* Identification of genes periodically expressed in the human cell cycle and their expression in tumours. *Mol. Biol. Cell* **13,** 1977–2000 (2002).
50. Skoufias, D. A. *et al.* S-trityl-L-cysteine is a reversible, tight binding inhibitor of the human kinesin Eg5 that specifically blocks mitotic progression. *J. Biol. Chem.* **281,** 17559–17569 (2006).
51. Kittler, R. *et al.* Genome-wide resources of endoribonuclease-prepared short interfering RNAs for specific loss-of-function studies. *Nat. Methods* **4,** 337–344 (2007).
52. Ganem, N. J. & Compton, D. A. The KinI kinesin Kif2a is required for bipolar spindle assembly through a functional relationship with MCAK. *J. Cell Biol.* **166,** 473–478 (2004).
53. Nagaraj, N. *et al.* Deep proteome and transcriptome mapping of a human cancer cell line. *Mol. Syst. Biol.* **7,** 548 (2011).
54. Wu, C. *et al.* BioGPS: an extensible and customizable portal for querying and organizing gene annotation resources. *Genome Biol.* **10,** R130 (2009).
55. Barrett, T. & Edgar, R. Gene expression omnibus: microarray data storage, submission, retrieval, and analysis. *Methods Enzymol.* **411,** 352–369 (2006).
56. Cheeseman, I. M. & Desai, A. A combined approach for the localization and tandem affinity purification of protein complexes from metazoans. *Sci. STKE* **266,** pl1 (2005).
57. Hales, C. N. & Woodhead, J. S. Labeled antibodies and their use in the immunoradiometric assay. *Methods Enzymol.* **70,** 334–355 (1980).
58. SPCTools, S.R.-S.a.S.R.-. http://tools.proteomecenter.org/wiki/index.php?title=Software:ReAdW.
59. Keller, A., Eng, J., Zhang, N., Li, X. J. & Aebersold, R. A uniform proteomics MS/MS analysis platform using open XML file formats. *Mol. Syst. Biol.* **1,** 20050017 (2005).
60. Mueller, L. N. *et al.* SuperHirn—a novel tool for high resolution LC-MS-based peptide/protein profiling. *Proteomics* **7,** 3470–3480 (2007).
61. Stark, C. *et al.* The BioGRID Interaction Database: 2011 update. *Nucl. Acids Res.* **39,** D698-D704 (2011).

DOI: 10.1038/ncb2689

nature cell biology

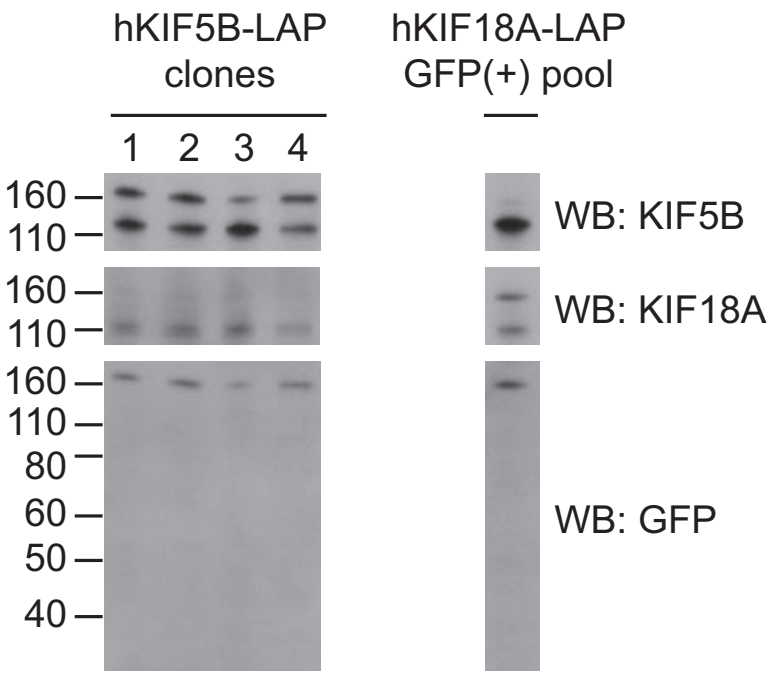

Figure S1 Wild-type expression levels of human BAC motors in HeLa. Western blot of lysates from FACS-sorted HeLa hKIF5B clones or a FACS-sorted GFP-positive hKIF18A HeLa BAC pool.

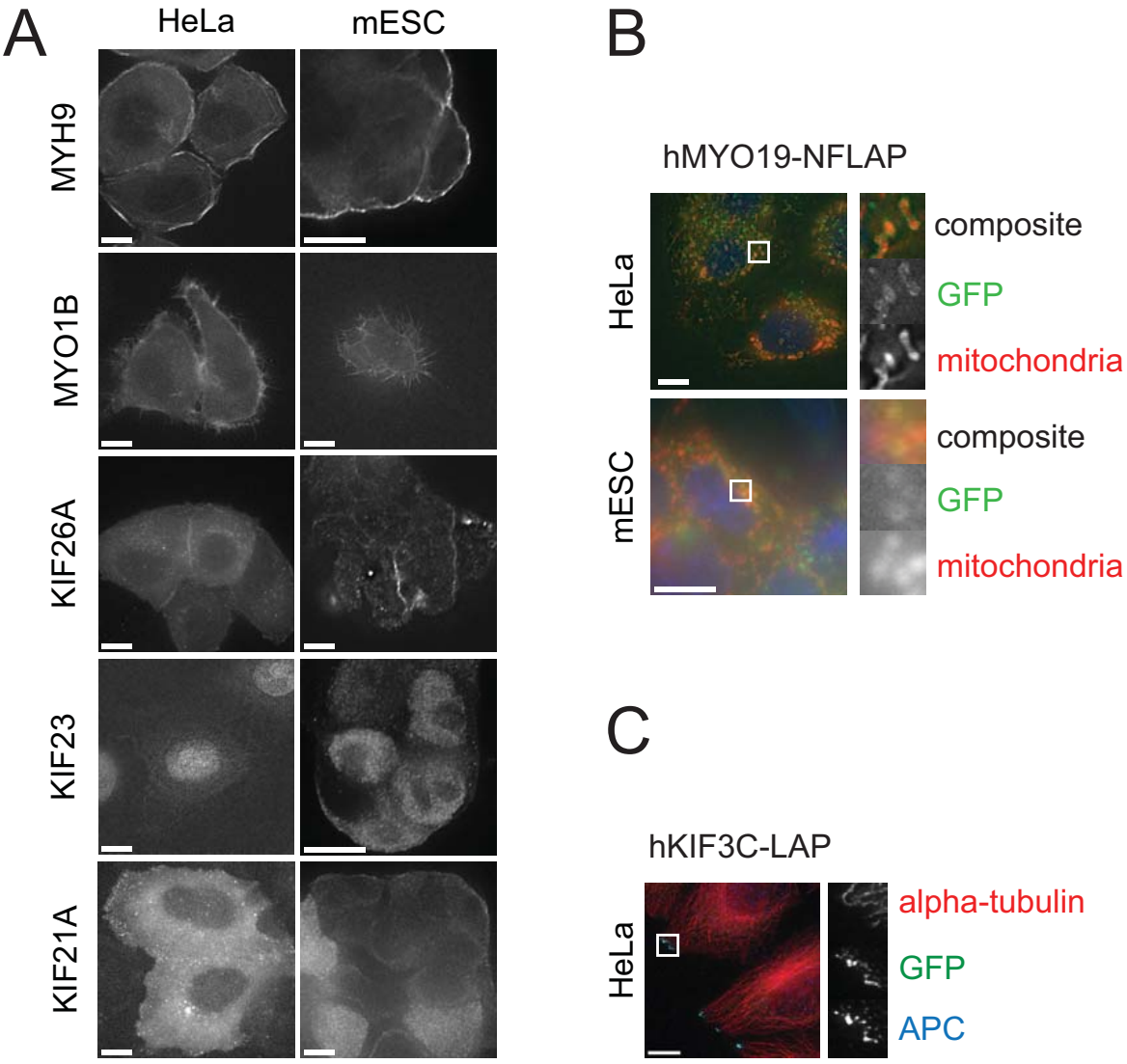

Figure S2 Motor targeting in transgenic HeLa and mESCs. **A.** GFP-immunostained images of fixed BAC HeLa (hMYH9-LAP, mMYO1B-LAP, hKIF26A-LAP, hKIF23-EGFP and hKIF21A-LAP) or mESC (mMYH9-NFLAP, mMYO1B-LAP, hKIF26A-LAP, hKIF23-EGFP and hKIF21A-LAP). Scale bars, 10 μm. **B.** Images of HeLa and mESCs expressing hMYO19-NFLAP stained for DNA (blue), GFP (green) and mitochondria (red). Inset, magnified (3x) images present composite, GFP and mitochondrial staining. Scale bars, 10 μm. **C.** HeLa BAC hKIF3C-LAP line stained for alpha-tubulin (red), GFP (green) and *adenomatous polyposis coli* (APC, blue). Inset, magnified (3x) images present grayscale images for each channel. Scale bar, 10 μm.

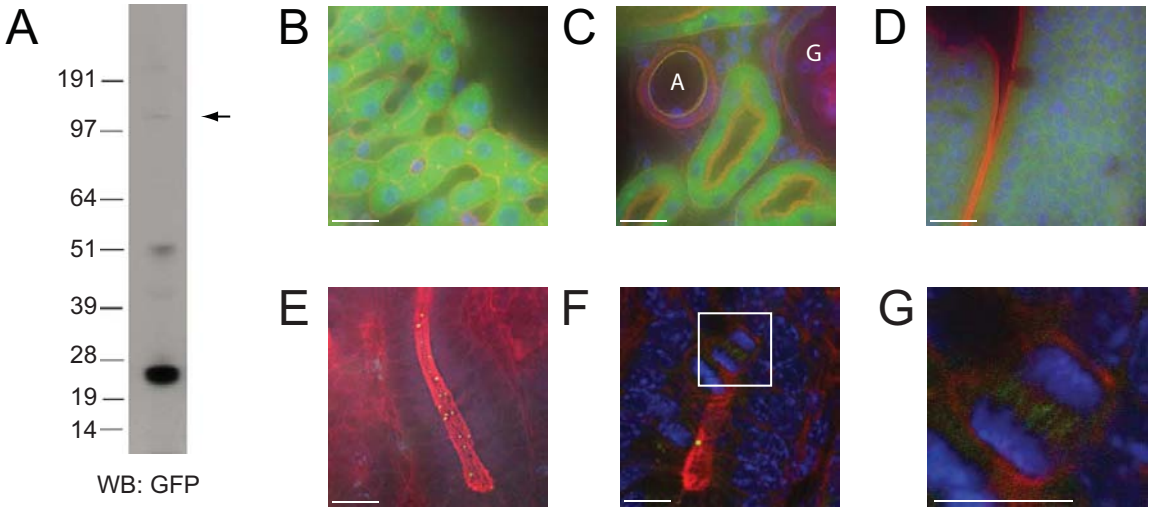

Figure S3 Characterization of a KIF23-EGFP transgenic mouse. **A.** Anti-GFP Western blot of femoral bone marrow from a 32 week-old female. The expected position for the KIF23 transgene (arrow, 105 kDa) is indicated. **B-D.** Deconvolved image projections of fixed tissue sections, including **B.** liver, **C.** kidney with labeled artery (A) and glomerulus (G) and **D.** absorptive intestinal epithelia stained for DNA (blue), filamentous actin (red) and GFP (green). Scale bar, 20 μm. **E.** Fixed thick section of intestinal crypt stained for *adenomatous polyposis coli* (blue), F-actin (red) and GFP (green). Scale bar, 20 μm. **F.** Intestinal crypt stained for DNA (blue) and filamentous actin (red) with native GFP fluorescence. Scale bar, 10 μm. **G.** Magnified (3x) image of anaphase cell in panel F inset. Scale bar, 10 μm.

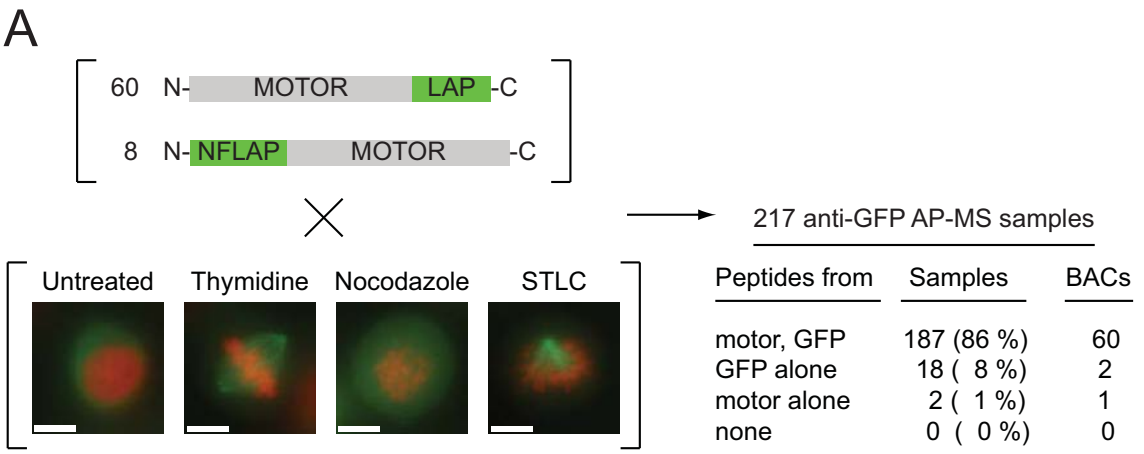

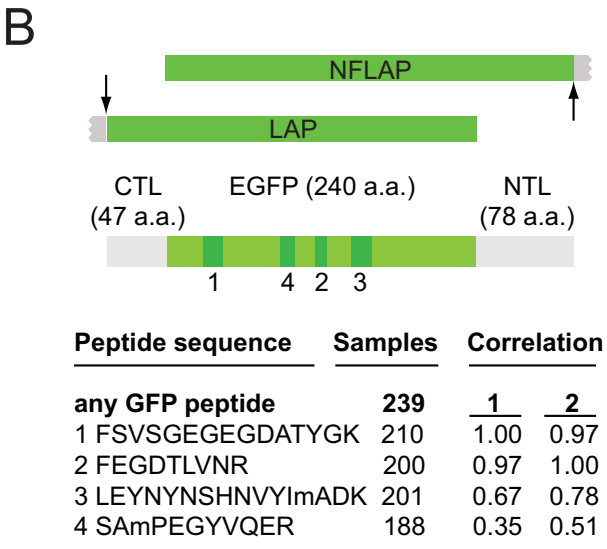

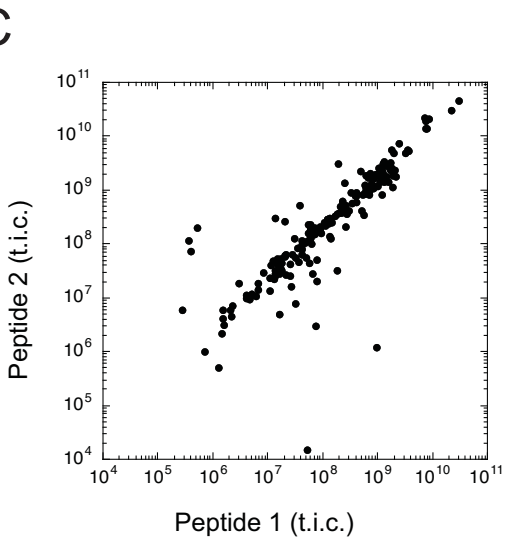

Figure S4 Quantitative AP-MS of BAC transgenes from HeLa. **A.** Summary of anti-GFP AP-MS screen from HeLa BAC pools. HeLa expressing one of 60 C- or 8 N-terminally tagged motor genes were harvested after culture in medium alone or following one of 3 mitotic enrichment protocols. Below, deconvolved image projections of live HeLa expressing alpha-tubulin-GFP (green) and mCherry-Histone 2B (red) are presented for each treatment. Scale bar, 10 μm. Right, tabulated success rate for identification of GFP and expected motor protein in 217 (80% of transgene-treatment combinations) AP-MS experiments (see Supplementary Information, Table S3). **B.** A cartoon map of recombinant C-terminal LAP and N-terminal NFLAP tags containing a core GFP domain (light green) and the four most abundant GFP-derived peptides (green) found in 250 total AP-MS experiments. The amino acid sequence ("m" is oxidized methionine), detection frequency and intensity (total ion count) cross-correlation with peptides 1 and 2 are presented. **C.** Total ion counts for GFP-derived peptides 1 and 2 in 200 samples (Correlation = 0.97).

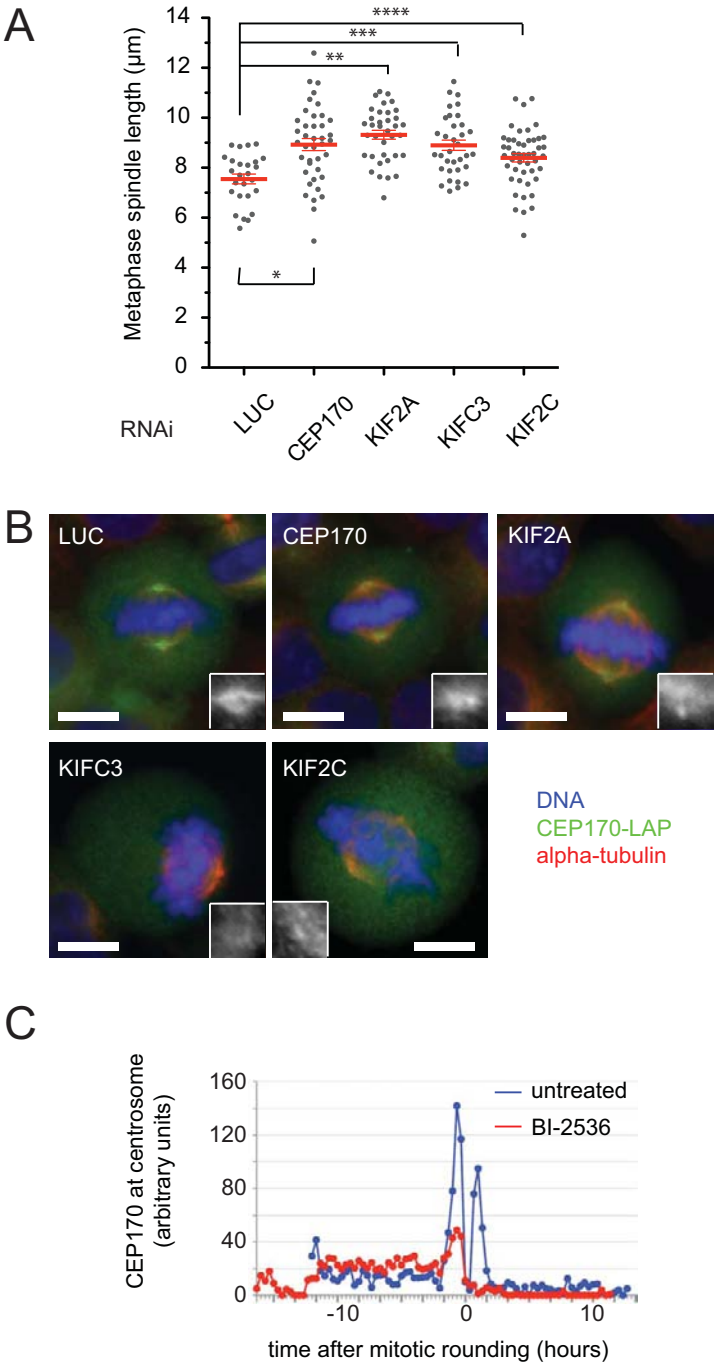

Figure S5 Regulation of CEP170 targeting to centrosomes. **A.** Metaphase spindle length measured in fixed HeLa treated with esiRNA. Bars: s.d.; *P=0.0001 (n=40 cells); ** P<0.0001 (n=36 cells); ***P=0.0001 (n=34 cells); ****P=0.0017 (n=47 cells) (Student's t-test). **B.** Representative metaphase images of the mCEP170-LAP HeLa BAC line following esiRNA targeting the genes, as noted, and stained for DNA (blue), GFP (green) and alpha-tubulin (red). Inset, grayscale images of GFP channel at representative microtubule spindle pole. Scale bars, 10 µm. **C.** Average (n=5 cells) measured GFP intensity at centrosomes of mCEP170-LAP in live HeLa cultured in the presence of 100 nM BI-2536 (red) or medium alone (blue).

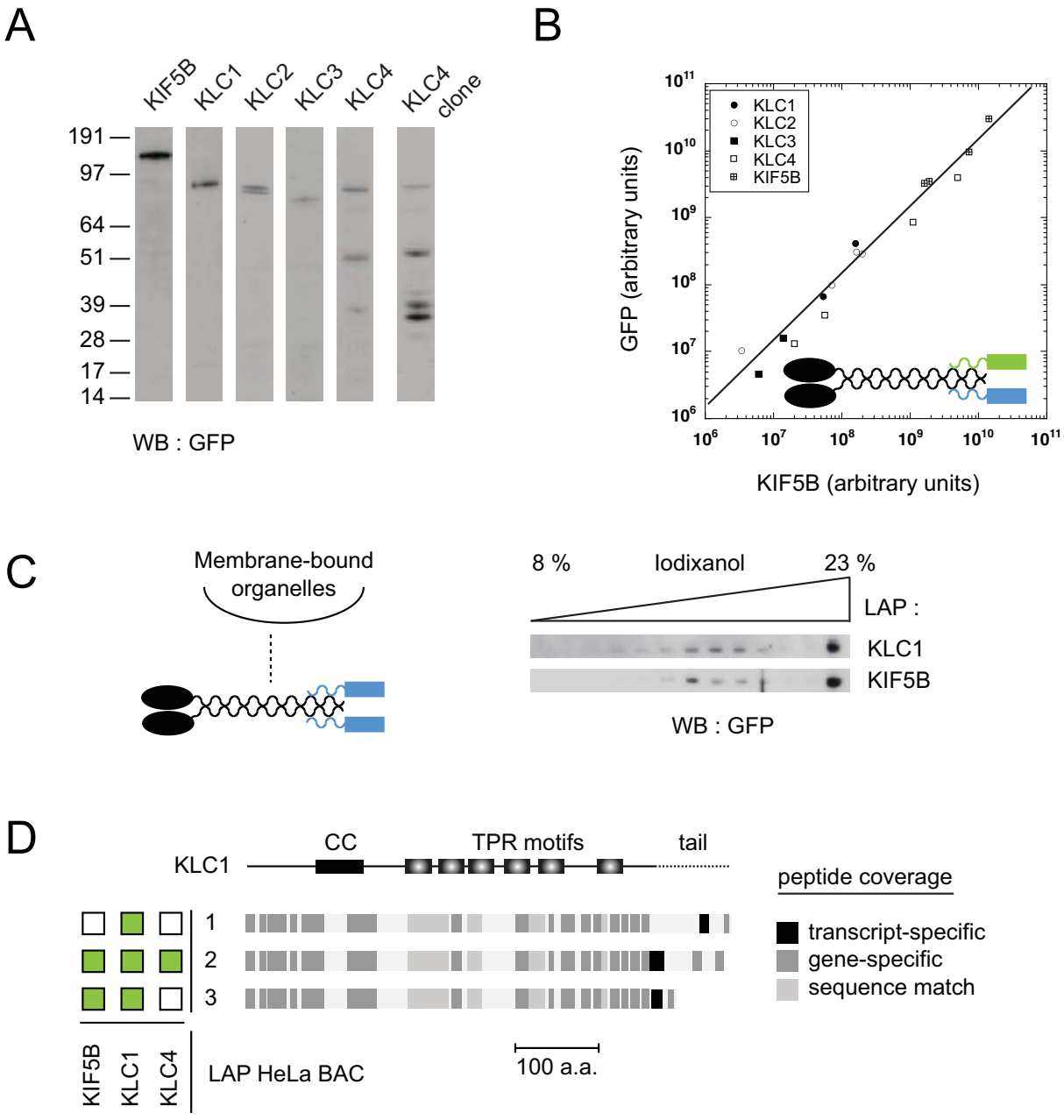

Figure S6 Biochemical analysis of conventional kinesin. **A.** Western blot of cell lysate from HeLa BAC pools expressing KIF5B-LAP, individual LAP-tagged KLCs or a clonal HeLa BAC line expressing hKLC4-LAP. **B.** Normalized spectral counts for abundant KIF5B and GFP-derived peptides in each AP-MS sample recovered with the following transgenes: KLC1 (filled circle), KLC2 (open circle), KLC3 (filled square), KLC4 (open square) and KIF5B (grid). Data fits a linear model (correlation = 0.91). The inset cartoon illustrates scenario for capture of conventional kinesin with recombinant (green) KLC and native KLC (blue) and KIF5B (black). **C.** Iodixanol density gradient centrifugation of microsomes purified from lysates of KIF5B-LAP or KLC1-LAP HeLa BAC lines. Western blot of the density fractions reveals a fraction of recombinant KLC and KIF5B binds membranes. **D.** The KLC1 splice isoforms contain a N-terminal coiled coil, a tetratricopeptide repeat (TPR) bundle and an isoform-specific C-terminal tail[46]. Below, peptide coverage maps for three KLC1 isoforms (1-3, respectively, ENSP00000334523, ENSP00000334618 and ENSP00000402779) detected in this study based on isoform-specific C-terminal peptides. Shading for the peptide overlap region indicates the degree of sequence selectivity; low (sequence match), medium (gene specific) and high (transcript-specific). Recovery of each KLC1 isoform by recombinant KIF5B, KLC1 and KLC4 are indicated (green), left.

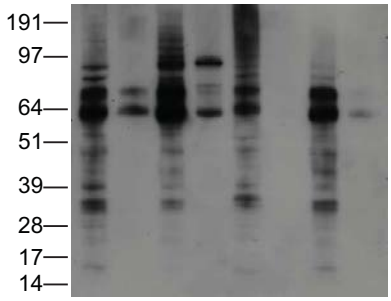

(Figure 7B and 7C, anti-KLC1)

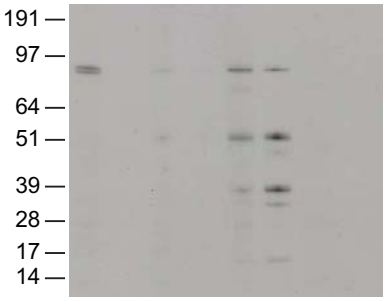

(Figure 7C, anti-GFP)
(Supplemental Information, Fig. S5A, anti-GFP)

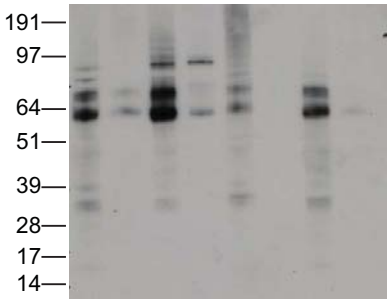

(Figure 7B and 7C, anti-KLC1)

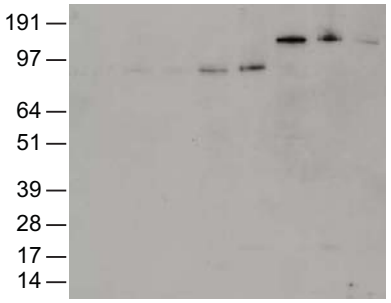

(Supplemental Information, Figure S5A, anti-GFP)

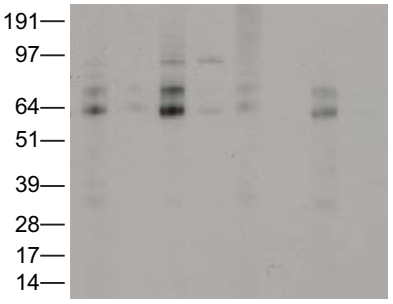

(Figure 7B, anti-KLC1)

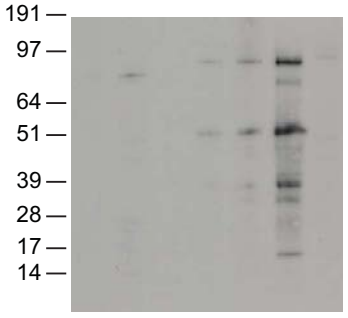

(Supplemental Information, Figure S5A, anti-GFP)

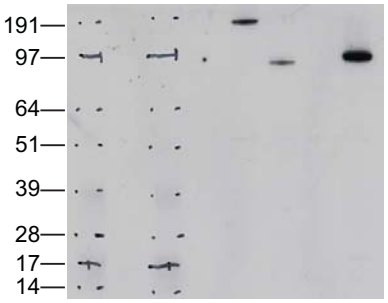

(Figure 7B, anti-GFP)

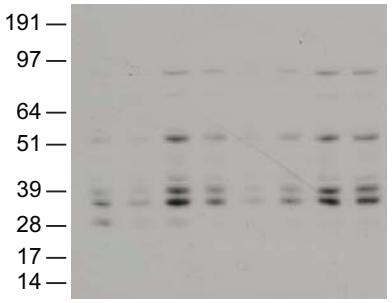

(Supplemental Information, Figure S5A, anti-GFP)

Figure S7 Original blots. Full Western blots used to prepare figures, as indicated.

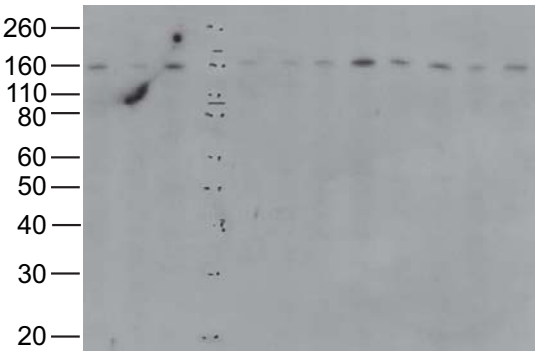

(Supplemental Information, Fig. S1, anti-GFP)

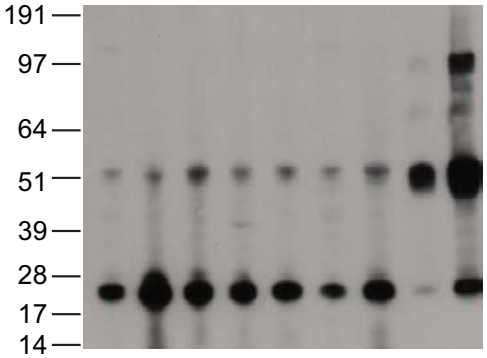

(Supplemental Information, Fig. S2)

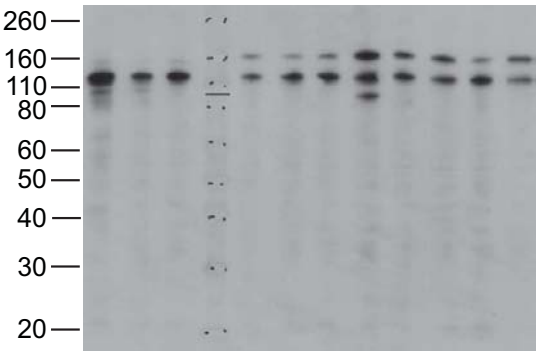

(Supplemental Information, Fig. S1, anti-KIF5B)

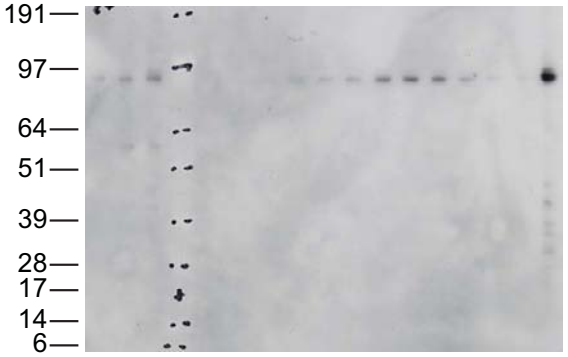

(Supplemental Information, Fig. S5C, KLC1)

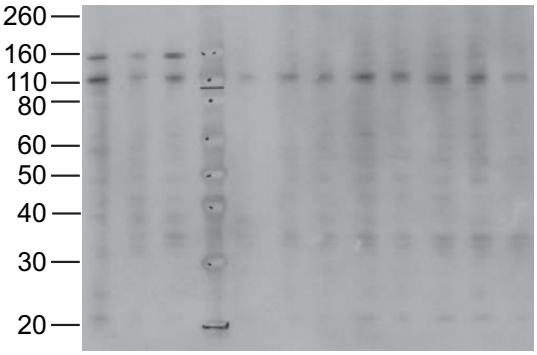

(Supplemental Information, Fig. S1, anti-KIF18A)

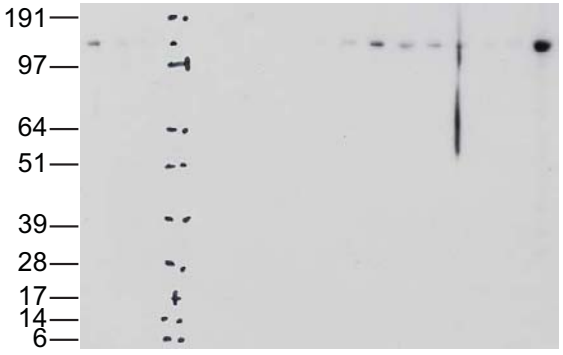

(Supplemental Information, Fig. S5C, KIF5B)

Figure S7 continued

Supplementary Table Legends

Table S1 Motor and kinesin light chain gene expression in human cells. A summary of motor gene expression data in HeLa and immune cells based on quantile-normalized microarray data in biological triplicate and bioinformatics, as described (see Supplementary Information, Methods). For each human gene (Gene Symbol), we indicate the ENSEBML gene ID (ENSEMBL), most informative Agilent microarray probe (Probe), and if that gene is expressed in HeLa, primary (pCD4N) or stimulated (sCD4N) naïve CD4+ T-lymphocytes, monocytes (MC), dendritic cells (DC) and macrophages (MP). The criteria for determination of expression in HeLa and immune lines is indicated as follows: published RNASeq and deep proteome of HeLa cells[47] (RNASeq/Proteome), true negative in HeLa based on microarray detection of heterologous BAC transgene (MA), comparison between HeLa and immune cells (Tissues), and selected references (PMID).

Table S2 Summary of BAC tagging and recombinant transgene access. For each combination of human kinesins, myosins and their mouse orthologs, we provide the following information: Organism (mouse or human), Gene name, Ensembl ID number, the C- or N-terminal tag and the tagged BAC transgene Reference Number for ordering as part of this BAC resource. Finally, we indicate if the PCR-verified recombinant transgene is available in this collection, if tagging failed or if the BAC was not commercially available.

Table S3 Cell transfection, characterization and cell line resource information. A summary of transgenic HeLa and mESC BAC lines generated as part of the motor protein resource. For each HeLa or mESC BAC pool, the cell type, gene name, recombinant tag, transgene number (as Supplementary Information, Table S2) and previous publication (Pubmed ID: PMID) of a given cell line. Western blot (WB) of each HeLa pool is annotated as follows; ns (no signal), est (expected molecular weight), truncated (molecular weight lower than expected), multiple (multiple bands). Localization by IFM during interphase (IFM-INT), prometaphase to metaphase (IFM-MIT) and anaphase to telophase (IFM-CYK) are annotated as follows; ns (no signal), CYT (cytoplasmic), DNA (nuclear or mitotic DNA), KT (kinetochores), MZ (anaphase spindle midzone), MB (midbody), CEN (centrosome), SP (mitotic or anaphase spindle), COR (cell cortex), RET (reticulum), NBOD (interphase nuclear body), EXT (cell extensions), PUN (puncta), ACT (actin-like: cortex and stress fibers), NE (nuclear envelope) and MITO (mitochondria).

Table S4 Recombinant proteins identified by AP-MS from HeLa BAC lysates. Summary of BAC transgene recovery in AP-MS experiments from clarified lysates (protocol: soluble) or adsorbed vesicles following non-specific acid (protocol: vesicle-acid) or specific TEV protease-mediated (protocol: vesicle-TEV) release. For each HeLa BAC pool, the relevant genome for BAC preparation, motor Gene name, tag and MCB reference number are provided, consistent with (see Supplementary Materials, Tables S2 and S3). Threshold for detection of thee expected motor protein (Bait) or recombinant tag (Tag) was at least 2 bait or tag-specific peptides from all AP-MS samples obtained using a HeLa BAC pool. Sequence coverage for each transgene was calculated using the longest Ensembl transcript as a reference. The total number of unique bait (transgene) and tag-derived peptides is noted for all the experiments. The remaining fields are indicated ns (no sample), or note the number of unique bait and tag-derived peptides is also noted for individual samples from U (cycling), T (thymidine-synchronized), N (nocodazole arrested) and S (STLC arrested) cells.

Table S5 Protein-protein interactions identified by AP-MS from HeLa BAC. The table identifies each bait transgene, the ENSEMBL ID and common name of the captured prey protein. Validation criteria include the Pubmed ID numbers for publications that report physical interaction, association by homology or functional genetic interactions, or co-localization. The total number of AP-MS samples positive for the interaction are indicated, followed by the number of prey-specific peptides identified for each individual sample, as follows, "2259U_7", indicates that 7 unique prey peptides were identified in lysate from cell line MCB2259 and treatment U. Data for both N- and C-terminally tagged alleles for each bait protein is included.

Table S6 Flanking sequences used to generate esiRNA. List of forward and reverse gene-specific flanking primers used to generate endonuclease-prepared siRNAs targeting human kinesins and CEP170 in this report.

Table S7 Summary of transcription profiles deposited in the Gene Expression Omnibus (GEO). Accession numbers and sample descriptions for each microarray profile available online at the Gene Expression Omnibus (GEO)[48] of the Nation Center for Biotechnology Information (NCBI) website.

Table S8 Online accession information for HeLa BAC images.
Cell Image Library (CIL) reference numbers for live or fixed-cell HeLa BAC images accessible online at The Cell: An Image Library (http://www.cellimagelibrary.org/).

Supplementary Video Legends

Video 1 HeLa BAC line expressing human KIF22-LAP.
Time-lapse (36 hours, 2 frames/hour) GFP fluorescence imaging of human KIF22-LAP expressed in a stable HeLa BAC line.

Video 2 HeLa BAC line expressing mouse KIF22-LAP.
Time-lapse (5 hours, 2 frames/hour) GFP fluorescence imaging of mouse KIF22-LAP expressed in a stable HeLa BAC line.

Video 3. HeLa BAC line expressing human KIF3C-LAP.
Time-lapse (15 hours, 3 frames/hour) GFP fluorescence imaging of human KIF3C-LAP expressed in a stable HeLa BAC line.

Video 4. Mouse embryonic stem cell BAC line expressing mouse KIF3A-NFLAP.
Time-lapse (2 min, 20 frames/min) GFP fluorescence imaging of human KIF3A-NFLAP expressed in stably transfected mouse embryonic stem cells.

Video 5. HeLa BAC line expressing mouse CEP170-LAP.
Time-lapse (16 hours, 3 frames/hour) GFP fluorescence imaging of mouse CEP170-LAP expressed in a stable HeLa BAC line.